Inferring Multi-Organ Genetic Causal Connections using Imaging and Clinical Data through Mendelian Randomization

Running title: MR atlas for multi-organ images

Juan Shu[1], Rong Zheng[2], Carlos Copana[1], Bingxuan Li[3], Zirui Fan[1,4], Xiaochen Yang[1], Yilin Yang[5], Xiyao Wang[3], Yujue Li[1], Bowei Xi[1], Tengfei Li[6,7], Hongtu Zhu[8,9,10,11]*, and Bingxin Zhao[1,4]*

[1]Department of Statistics, Purdue University, West Lafayette, IN 47907, USA.
[2]Department of Nuclear Medicine, First Hospital of Shanxi Medical University, Taiyuan, Shanxi 030001, China.
[3]Department of Computer Science, Purdue University, West Lafayette, IN 47907, USA.
[4]Department of Statistics and Data Science, University of Pennsylvania, Philadelphia, PA 19104, USA.
[5]Department of Computer and Information Science and Electrical and Systems Engineering, School of Engineering & Applied Science, University of Pennsylvania, Philadelphia, PA 19104, USA.
[6]Department of Radiology, University of North Carolina at Chapel Hill, Chapel Hill, NC 27599, USA.
[7]Biomedical Research Imaging Center, School of Medicine, University of North Carolina at Chapel Hill, Chapel Hill, NC 27599, USA.
[8]Department of Biostatistics, University of North Carolina at Chapel Hill, Chapel Hill, NC 27599, USA.
[9]Department of Genetics, University of North Carolina at Chapel Hill, Chapel Hill, NC 27599, USA.
[10]Department of Computer Science, University of North Carolina at Chapel Hill, Chapel Hill, NC 27599, USA.
[11]Department of Statistics and Operations Research, University of North Carolina at Chapel Hill, Chapel Hill, NC 27599, USA.

**Corresponding authors*:
Hongtu Zhu
3105C McGavran-Greenberg Hall, 135 Dauer Drive, Chapel Hill, NC 27599.
E-mail address: htzhu@email.unc.edu Phone: (919) 966-7250

Bingxin Zhao
413 Academic Research Building, 265 South 37th Street, Philadelphia, PA 19104.
E-mail address: bxzhao@upenn.edu Phone: (215) 898-8222

Abstract

Deciphering the complex causal relationships between multiple organs and major clinical outcomes and the causal interplay among multiple organs remains a significant challenge. By utilizing imaging biomarkers, we can characterize the functional and structural architectures of major human organs. Mendelian randomization (MR) provides a valuable framework for inferring causality by leveraging genetic variants as instrumental variables. In this study, we conducted a systematic multi-organ MR analysis involving 402 imaging biomarkers and 88 clinical outcomes. Our analysis revealed 488 genetic causal links for 62 diseases and 130 imaging biomarkers across various organs, tissues, and systems, including the brain, heart, liver, kidney, lung, pancreas, spleen, adipose tissue, and skeletal system. We specifically focused on critical intra-organ causal connections, such as the bidirectional genetic links between Alzheimer's disease and brain function, as well as inter-organ causal effects, such as the detrimental impact of heart diseases on brain health. These findings shed light on the genetic causal links spanning multiple organs, contributing to a deeper understanding of the intricate relationships between organ imaging biomarkers and clinical outcomes. Our multi-organ MR results can be explored at https://mr4mo.org/.

Keywords: Brain imaging; Clinical outcomes; FinnGen; GWAS; Heart imaging; Mendelian randomization; MRI; Organ imaging; UK Biobank.

Medical imaging techniques such as magnetic resonance imaging (MRI) measure the structure and function of many human organs, such as the brain, heart, liver, and kidney. Their derived imaging biomarkers have found widespread use in both clinical research and practical applications. For example, structural and functional imaging biomarkers extracted from brain MRIs have consistently revealed abnormalities associated with Alzheimer's disease, particularly within the hippocampal region[1]. Cardiovascular MRI (CMR) provides insights into changes in ventricular function, cardiovascular structure, and myocardial perfusion, all of which are intricately linked to cardiovascular diseases[2]. Furthermore, skeletal Dual-Energy X-ray Absorptiometry (DXA) aids in identifying novel genetic variants that influence the human skeletal structure, thereby revealing significant evolutionary trends in human anatomical changes leading to pathogenesis[3]. Several large-scale organ imaging datasets (on the scale of over 10,000 participants) have recently been made publicly available, revealing details about human organ structure and function[4-8]. A multitude of complex traits and clinical outcomes have been found to associate with organ imaging biomarkers, as evidenced by these robust, population-based studies[9,10]. Despite these advances, inherent limitations in observational data pose challenges in definitively establishing causal relationships between imaging biomarkers and clinical outcomes, as well as in gaining a comprehensive understanding of the causal interplay across various organs[11]. Mendelian randomization (MR) utilizes genetic variants as instrumental variables to infer causality from observational data[12,13]. Operating under certain assumptions regarding genetic, exposure, and outcome variables, MR seeks to uncover causal relationships between exposure and outcome variables, while controlling for confounding factors. Both family and population-based studies have demonstrated that numerous imaging biomarkers and complex diseases are profoundly influenced by genetics. Hundreds of associated genetic loci have been pinpointed in large-scale genome-wide association studies (GWAS)[8,14-29]. By utilizing these GWAS summary-level data (summary statistics), MR methods can unveil causal relationships between imaging measurements and clinical outcomes. Numerous recent MR studies have explored the genetic causality of imaging biomarkers[11,30-35]. However, a common limitation of these MR studies is their focus on a single organ (or imaging modality) and/or a single disease, or diseases in a specific domain, such as brain imaging and psychiatric disorders[30]. It is crucial to note, though, that many diseases act as the causes and/or consequences of

functional and structural changes in various organs of the human body. Cross-organ analysis can elucidate the complexity of human physiology, subsequently improving our capacity to diagnose, treat, and prevent a multitude of diseases. Consequently, it is essential to conduct MR analysis from a multi-organ perspective to comprehend the clinical implications of imaging biomarkers amidst the complex interrelationships of organ systems.

In this paper, we carried out a systematic two-sample MR analysis to explore the causal relationships between multi-organ imaging and clinical endpoints. We consolidated GWAS summary statistics from 402 multi-organ imaging biomarkers (with an average sample size $n \approx 35{,}000$) from the UK Biobank (UKB)[36] study along with 88 clinical outcomes (each with more than 10,000 cases) sourced from the FinnGen project[27] (**Fig. S1** and **Tables S1-S2**). Our focus was on three major brain MRI modalities: 1) 101 regional brain volumes[21] from structural MRI (sMRI); 2) 110 diffusion tensor imaging (DTI) parameters[23] from diffusion MRI (dMRI); and 3) 90 functional activity (amplitude[37]) and connectivity traits from functional MRI (fMRI)[25]. Furthermore, we incorporated 82 CMR traits extracted from short-axis, long-axis, and aortic cine cardiac MRI[38,39]. We also considered 11 abdominal MRI biomarkers, measuring volume, fat, or iron content in seven organs and tissues[8], and eight DXA imaging biomarkers that gauged the lengths of all long bones and the width of the hip and shoulder[29]. We applied 8 MR methods[40-48] to investigate bidirectional genetic causal links. The study design is presented in **Figure 1A,** while **Figure 1B** offers a high-level summary of our key findings. Additional details on these multi-organ imaging biomarkers are provided in the Methods section. We have made our database publicly available and developed a browser framework to facilitate the exploration of multi-organ MR findings (http://mr4mo.org/).

RESULTS

Genetic causality between brain imaging and multi-organ diseases

We explored the causal relationship between brain imaging biomarkers and multi-organ diseases. At the Bonferroni significance level ($P < 5.18\times10^{-6}$, multiple testing adjustment for both directions), MR highlighted 127 significant genetic causal effects on 58 brain imaging biomarkers stemming from 20 diseases in 8 major categories. These categories

include mental and behavioral disorders, diseases of the nervous system, diseases of the circulatory system, cardiometabolic endpoints, interstitial lung disease endpoints, diseases marked as autoimmune origin, diseases of the eye and adnexa, and diseases of the genitourinary system (**Fig. S2** and **Table S3**). Heart-related diseases were the most frequent (66/127) and were predominantly linked to DTI parameters and a smaller set of regional brain volumes. We did not observe significant causal effects from heart diseases to fMRI traits. The top three heart diseases demonstrating causal genetic influences on brain structures were peripheral artery disease (15/66), hypertension (14/66), and hypertensive diseases (12/66) (**Figs. S2-S4**). For example, peripheral artery disease causally impacted the white matter microstructure within the anterior limb of the internal capsule (ALIC, $|\beta|>0.15$, $P < 3.04\times10^{-8}$), the body of corpus callosum tract (BCC, $|\beta|>0.14$, $P < 8.44\times10^{-7}$), and the genu of corpus callosum tract (GCC, $|\beta|>0.13$, $P < 4.24\times10^{-6}$). Hypertension and hypertensive diseases causally affected the superior corona radiata (SCR, $|\beta|>0.07$, $P < 9.47\times10^{-8}$). Beyond DTI parameters, hypertension also negatively impacted the total grey matter volume ($|\beta|>0.02$, $P < 1.26\times10^{-8}$) (**Figs. 2C** and **S2-S3**). In addition to heart-related diseases, several other non-neurological clinical endpoints also influenced brain health. For example, asthma had negative causal effects on the SCR ($|\beta|>0.05$, $P < 7.26\times10^{-7}$) and the volume of the right inferior lateral ventricle ($|\beta|>0.09$, $P < 8.66\times10^{-7}$) (**Fig. S5**).

Brain disorders also demonstrated causal effects on brain imaging biomarkers (49/127), with dementia and Alzheimer's disease emerging as the most common brain-related diseases (**Fig. S2**). Intriguingly, brain disorders are primarily linked to fMRI traits. For example, Alzheimer's disease consistently exhibited a causal relationship with decreased functional activity in the dorsal attention ($|\beta|>0.04$, $P < 5.07\times10^{-8}$), frontoparietal, and secondary visual network ($|\beta|>0.04$, $P < 4.70\times10^{-8}$), as well as DTI parameters of the SCR ($|\beta|>0.03$, $P < 1.85\times10^{-6}$) (**Figs. 2A** and **S6**). Both functional MRI and DTI parameters have been widely used in Alzheimer's disease research[49]. White matter abnormalities, such as those in the left SCR, and decreased functional connectivity in attention-related networks, have been identified in patients with Alzheimer's disease[50,51]. Similar to Alzheimer's disease, dementia showed negative causal genetic effects on functional activity in multiple networks, including the cingulo-opercular, default mode, dorsal attention,

frontoparietal, language, posterior multimodal, and secondary visual networks (|β|>0.12, $P < 4.74\times10^{-8}$) (**Figs. 2B** and **S7**). Additionally, mood disorders affected brain volume traits, such as the left and right putamen (|β|>0.04, $P < 5.64\times10^{-7}$) (**Fig. S8**). A more comprehensive summary of causal genetic links from clinical endpoints to brain imaging biomarkers can be found in **Figures S3-S9**.

Brain and other organ-related diseases may also be caused by structural or functional changes in the brain. To investigate this, we used brain imaging biomarkers as exposure variables and clinical endpoints as the outcome variables. At the Bonferroni significance level ($P < 5.18\times10^{-6}$), we identified 85 significant relationships between 22 brain imaging biomarkers and 20 clinical endpoints (**Fig. S10** and **Table S3**). Most of the significant imaging-disease pairs were related to fMRI traits. Specifically, 66 of the 85 pairs were linked to fMRI traits, 10 to DTI parameters, and 9 to regional brain volumes. The majority of the significant findings pertained to brain diseases (65/85), with a minor proportion linked to heart diseases (13/85), autoimmune diseases (4/85), COPD and related endpoints (1/85), diseases of the eye and adnexa (1/85), and diseases of the genitourinary system (1/85). For example, we found that reduced activity in several functional networks correlated with an increased risk of Alzheimer's disease, such as the default mode and dorsal-attention networks (|β|>0.5, $P < 5.65\times10^{-13}$) (**Figs. 3A** and **S11**). Additionally, genetic causal effects from DTI parameters on Alzheimer's disease were identified, such as those related to the BCC and SCR (|β|>0.49, $P < 6.79\times10^{-7}$) (**Figs. 3A** and **S11**).

Dementia exhibited a pattern similar to Alzheimer's disease, being causally influenced by decreased activity in multiple networks, such as the default mode, dorsal-attention, and secondary visual network (|β|>0.002, $P < 2.77\times10^{-7}$) (**Fig. 3B** and **S12**). Other brain diseases, such as neuropsychiatric disorders (|β|>0.09, $P<8.88\times10^{-16}$) and neurological diseases (|β|>0.06, $P < 1.72\times10^{-6}$) were also found to be causally linked to fMRI traits, including the functional activity of the secondary visual network and functional connectivity of the default mode network (**Figs. S13** and **S14**). Finally, we discovered that alterations in brain structure may also impact other non-neurological diseases. For example, the left basal forebrain exhibited a negative causal effect on hypertensive diseases (|β|>0.12, $P < 8.47\times10^{-9}$) and hypertension (|β|>0.15, $P < 6.19\times10^{-11}$).

Additionally, the left lingual was found to negatively influence female genital prolapse ($|\beta|>0.75$, $P < 8.68\times10^{-7}$).

Causal genetic relationships between CMR traits and clinical outcomes

We first assessed the causal effects from clinical endpoints to CMR measures of heart structure and function. We identified 111 significant results at the Bonferroni significance level ($P < 6.85\times10^{-6}$), encompassing 41 unique CMR traits of the ascending aorta (AAo), descending aorta (DAo), left atrium (LA), and left ventricle (LV). These significant causal effects were identified from 13 unique clinical endpoints in three categories: diseases of the circulatory system (8/13), cardiometabolic endpoints (4/13), as well as COPD and related endpoints (1/13). Most significant findings were linked to heart-related diseases, with 66 out of 111 associated with diseases of the circulatory system and 44 out of 111 tied to cardiometabolic endpoints (**Fig. S15** and **Table S4**).

The most frequently occurring genetic effects were linked to hypertensive diseases and hypertension (**Figs. 4A** and **S16**). Specifically, hypertensive diseases exerted negative causal impacts on AAo and DAo distensibility ($|\beta|>0.10$, $P < 1.26\times10^{-7}$), associations of which have been identified in prior studies[52-54]. Hypertensive diseases also influenced LV and LA traits, such as the global radial strain ($|\beta|>0.06$, $P < 4.47\times10^{-9}$), LA stroke volume ($|\beta|>0.07$, $P < 3.04\times10^{-8}$), and LV myocardial mass ($|\beta|>0.11$, $P < 3.04\times10^{-15}$, and see **Fig. 4B**). These findings align with findings from previous genetic association studies[55,56]. Hypertension exhibited a similar pattern to hypertensive diseases, causing impacts on various AAo and DAo traits, like DAo distensibility, and LA and LV traits, such as the LA minimum volume (LA_{min} volume, $|\beta|>0.03$, $P < 7.11\times10^{-6}$, and see **Fig. 4C**).

Moreover, angina pectoris was found to causally influence the AAo maximum and minimum areas (AAo_{max} and AAo_{min} areas, $|\beta|>0.71$, $P < 1.44\times10^{-7}$). Aortic aneurysm positively affected the DAo maximum and minimum areas (DAo_{max} and DAo_{min} areas, $|\beta|>0.71$, $P < 1.63\times10^{-24}$) as well as AAo_{max} and AAo_{min} areas ($|\beta|>0.16$, $P < 2.22\times10^{-6}$), aligning with clinical observations. Atrial fibrillation and flutter primarily impacted LA traits, such as the LA ejection fraction ($|\beta|>0.07$, $P < 5.88\times10^{-8}$), LA maximum volume (LA_{max} volume, $|\beta|>0.07$, $P < 1.62\times10^{-6}$), and LA_{min} volume ($|\beta|>0.08$, $P < 8.26\times10^{-8}$). Notably, atrial fibrillation is often linked to a decrease in ejection fraction and an increase

in LA volumes[57,58]. Apart from heart-related diseases, COPD and related endpoints were found to influence CMR traits. Specifically, COPD had a negative effect on DAo_{max} area ($|\beta|>0.10$, $P < 4.45\times10^{-11}$, and see **Fig. S16**). Emphysema, a variant of COPD characterized by the deterioration of lung tissue, could contribute to the dilatation of the thoracic aorta[59]. This could be due to emphysema's role in damaging elastic fibers in the lungs, which could then lead to changes in the elasticity of the aortic wall[60]. Such alternations could cause the thoracic aorta to dilate or balloon, thus increasing the risk of both aortic aneurysm and abdominal aortic abnormalities[59]. These findings help elucidate the potential biological mechanisms driving these causal relationships.

Alternatively, structural and functional abnormalities within the heart may escalate the risk of multi-organ diseases, considering the heart's role in pumping blood to all other organs to sustain their functions[61]. We examined this direction by treating CMR traits as exposure variables and clinical endpoints as the outcomes. After Bonferroni adjustment ($P < 6.85\times10^{-6}$), we identified 27 significant causal pairs, 25 related to heart-related diseases and 2 to autoimmune diseases (**Figs. 4D-G, S17,** and **Table S4**). For example, the global peak circumferential strain was positively correlated with heart failure and antihypertensive medication use ($|\beta|>0.51$, $P < 8.49\times10^{-8}$), whereas the LV ejection fraction exerted a negative causal effect on these conditions ($|\beta|>0.55$, $P < 1.12\times10^{-6}$). In addition to heart-related diseases, heart structural alternations also influenced diseases of autoimmune origin. For example, the right ventricular end-systolic volume negatively affected autoimmune diseases as defined by FinnGen[27] ($|\beta|>0.18$, $P < 3.10\times10^{-6}$) (**Figs. 4D** and **S18**). In summary, we discovered causal relationships between CMR traits and heart-related diseases, which generally exhibited bidirectionality. Furthermore, we elucidated the inter-organ causal relationships between the heart and other organs.

Causal genetic links between abdominal imaging biomarkers and clinical outcomes

We first investigated the impact of multi-organ diseases on abdominal imaging biomarkers, encompassing the volume or iron content of organs like the spleen, kidney, liver, lung, and pancreas[8]. At the Bonferroni significance level ($P < 6.69\times10^{-5}$), we identified 51 significant causal pairs from multi-organ diseases to abdominal imaging biomarkers. Among these, liver imaging biomarkers were the most affected (26/51).

Brain-related diseases emerged as the most common in all significant findings (35/51), succeeded by heart-related diseases (7/51), rheumatoid endpoints (4/51), diseases of the eye and adnexa (3/51), and autoimmune diseases (2/51) (**Figs. 5A-E, S19,** and **Table S5**). These findings corroborated ongoing research concerning the interplay between the brain and abdominal organs, such as the brain-gut connection[62-64], brain-kidney connection[65,66], and brain-liver connection[67].

Alzheimer's disease and dementia were consistently observed to have causal relationships with various abdominal imaging biomarkers, such as the percent liver fat ($|\beta|>0.37$, $P < 4.96\times10^{-6}$), liver volume ($|\beta|>0.03$, $P < 5.88\times10^{-5}$), and adipose tissue measurement ($|\beta|>0.06$, $P < 3.13\times10^{-5}$, and see **Figs. 5A** and **5C**). Apart from Alzheimer's disease and dementia, several other brain-related diseases were found to potentially affect abdominal organs. These included mental and behavioral disorders due to alcohol and psychoactive substance use, and sleep apnoea. For example, sleep apnoea impacted various abdominal traits, such as the liver volume ($|\beta|>0.11$, $P < 2.80\times10^{-5}$) and kidney volume ($|\beta|>0.23$, $P < 2.57\times10^{-6}$, and see **Fig. 5B**). Sleep apnoea may contribute to renal damage via mechanisms such as ischemic stress, hemodynamic changes, or intermediary conditions like hypertension, which may result in early chronic kidney disease[68,69]. Several heart-related diseases also genetically influenced abdominal organs. For example, heart failure and the use of antihypertensive medication could lead to an increase in spleen volume ($|\beta|>0.004$, $P < 2.66\times10^{-6}$). It's well-established that heart splenic enlargement often results from blood stasis and right heart disease frequently coincides with splenomegaly[70]. Atherosclerosis was found to be causally linked to pancreas iron content, a finding also supported by clinical evidence[71,72].

Beyond brain and heart-related diseases, we also observed causal effects from other diseases, such as autoimmune diseases on spleen volume and liver iron content. The spleen, as the largest immune organ in the body, may become enlarged due to various rheumatic and immune system diseases including systemic lupus erythematosus, Felty's syndrome, sarcoidosis, and autoimmune hepatitis[73-76]. We found a causal connection between liver iron content and both autoimmune and rheumatological diseases ($|\beta|>0.10$, $P < 3.02\times10^{-5}$). Excessive iron ions have been observed to deposit in tissues

affected by autoimmune diseases, such as brain tissues of multiple sclerosis patients and the synovial fluid of patients with rheumatoid arthritis[77]. Additionally, we observed disorders of the choroid and retina, along with the eye and adnexa diseases, to be causally connected to liver iron content ($|\beta|>0.10$, $P < 6.48\times10^{-5}$, and refer to **Figs. 5A** and **S20**). Metal, including iron, tends to accumulate in human ocular tissues, notably in the choroid and retinal pigment epithelium[78].

Next, we tested the opposite direction that abdominal imaging biomarkers as exposure variables and multi-organ diseases as outcomes. At the Bonferroni significance level ($P < 6.69\times10^{-5}$), we identified 55 significant pairs, with heart-related diseases being the most common (34/55). These were followed by brain-related diseases (11/55), diseases marked as autoimmune origin (2/55), diseases of the eye and adnexa (5/55), and diseases of the genitourinary system (3/55) (**Figs. 5D-E, S21,** and **Table S5**). For example, pancreas fat was found to have a causal impact on deep vein thrombosis of the lower extremities and pulmonary embolism ($|\beta|>0.38$, $P < 1.04\times10^{-12}$). Reduction in pancreatic fat content might directly enhance cellular function and insulin secretion rate, which could influence triglyceride levels and blood flow[79]. Consequently, we found that larger liver, spleen, and kidney volumes were all causally linked to heart-related diseases (**Figs. 5D** and **S22**). Specifically, a larger liver volume was causally linked to hypertensive diseases and hypertension ($|\beta|>0.13$, $P < 1.19\times10^{-10}$); a larger kidney volume was causally related to an increased risk of stroke ($|\beta|>0.25$, $P < 3.33\times10^{-5}$); and a larger spleen volume had causal effects on a range of heart-related diseases, including coronary angioplasty ($|\beta|>0.14$, $P < 4.94\times10^{-7}$), coronary atherosclerosis ($|\beta|>0.07$, $P < 6.94\times10^{-10}$), and peripheral artery diseases ($|\beta|>0.21$, $P < 4.98\times10^{-5}$). Kidney diseases, especially nephrotic syndrome, often lead to thrombotic and embolic complications, increasing the risk of stroke, due to platelet over-activation and the use of diuretics and glucocorticoids that can exacerbate hypercoagulability[80-82]. For brain-related disorders, we observed causal effects from liver volume to alcohol use disorder, as well as mental and behavioral disorders due to alcohol and psychoactive substance use. In addition, percent liver fat was causally linked with Alzheimer's disease, dementia, and psychiatric diseases. Prior studies have reported that non-alcoholic fatty liver disease may contribute to neurological conditions such as cognitive impairment and memory loss via pathways of

insulin resistance, inflammation, and excessive cytokine secretion[83-86]. In conclusion, we found that brain-related disorders can lead to changes in abdominal organs, and that these bidirectional relationships are observed in both neurodegenerative and psychiatric disorders. Conversely, various abdominal organs were found to be causally linked to heart-related diseases.

Causal genetic links between skeleton DXA traits and clinical outcomes

We first identified the causal effects of multiple organ diseases on DXA-derived skeleton traits[3]. At the Bonferroni significance level ($P < 3.39\times10^{-5}$), we found compelling evidence that multi-organ diseases impacted human skeleton health. The majority of these diseases were heart-related diseases (6/12) and nervous system (4/12), with rheumatic disease (1/12) and diseases of the genitourinary system (1/12) also having an impact (**Fig. S23** and **Table S6**). Carpal tunnel syndrome ($|\beta|>0.0007$, $P < 6.25\times10^{-8}$) and sleep apnoea ($|\beta|>0.001$, $P < 6.35\times10^{-8}$) were causally related to a higher average forearm length. Carpal tunnel syndrome occurs when the median nerve, which extends from the forearm to the palm of the hand, is compressed, impacting the wrist-to-forearm ratio[87,88]. It has been observed that oral appliance therapy[89], an effective treatment of sleep apnea, is associated with skeletal changes[90]. Moreover, disorders of the nerve, nerve root, and plexus disorders were causally linked with higher average tibia length ($|\beta|>0.001$, $P < 2.78\times10^{-5}$), which aligns with the previous finding that a specific type of plexus disorder, the lumbosacral plexus disorder, is associated with the lower leg[91]. Heart-related diseases also had causal effects on several DXA traits. For example, coronary heart disease had a negative causal effect on average tibia length ($|\beta|>0.0002$, $P < 2.50\times10^{-5}$), and a positive causal effect on hip width ($|\beta|>0.0004$, $P < 1.68\times10^{-5}$). Additionally, gonarthrosis affected the average tibia length ($|\beta|>0.0005$, $P < 1.69\times10^{-5}$) (**Figs. 6A** and **S24**).

The skeletal system serves as the foundational support for the human body, and as such, skeletal abnormalities could potentially contribute to the risk of multi-organ diseases. We identified 17 causal pairs at the Bonferroni significance level ($P < 3.39\times10^{-5}$). Over half (10/17) of these results were related to the heart, with the remainder pertaining to rheumatic disease (3/17), diseases of the eye and adnexa (2/17), interstitial lung diseases (1/17), and diseases of the genitourinary system (1/17) (**Fig. S23** and **Table S6**). Average

tibia length was causally linked to coxarthrosis ($|\beta|$>30.03, $P < 3.11\times10^{-9}$), gonarthrosis ($|\beta|$>19.39, $P < 3.18\times10^{-7}$), and other rheumatological endpoints ($|\beta|$>13.12, $P < 2.74\times10^{-5}$). There is evidence that leg length discrepancy could lead to issues with lower limb biomechanics, such as gonarthrosis, coxarthrosis, and other lower limb symptoms[92,93]. Torso length was found to causally affect heart-related issues, such as coronary angioplasty ($|\beta|$>38.85, $P < 9.45\times10^{-5}$), coronary atherosclerosis ($|\beta|$>22.94, $P < 1.22\times10^{-5}$), hard cardiovascular diseases ($|\beta|$>18.12, $P<1.30\times10^{-5}$), and ischemic heart diseases ($|\beta|$>30.99, $P < 1.33\times10^{-5}$). Previous studies examining the relationship between skeletal length and heart diseases have primarily focused on leg length or overall body height, generally reporting negative associations[94,95]. Consistent with these associations, we found that a long torso can lead to a higher risk of heart disease. We also observed that a higher average tibia length is causally linked to a lower risk of hypertension ($|\beta|$>6.46, $P < 1.27\times10^{-7}$), which is in line with previous findings[96] (**Figs. 6B** and **S25**). In conclusion, we found that rheumatoid endpoints (such as gonarthrosis) and diseases of the nervous system (such as nerve, nerve root, and plexus disorders) had a significant impact on bone health. Conversely, skeletal traits, like torso length, demonstrated a causal link with heart diseases.

Discussion

Observational studies have identified numerous links between various imaging-derived phenotypes and clinical outcomes. However, these associations are often influenced by residual confounding, complicating the accurate inference of causal effect sizes [97]. MR allows for the inference of causal relationships between exposure and outcome variables. MR leverages the natural and random assortment of genetic variants during meiosis, making these variants ideal instrumental variables for discerning causal effects. In the present study, we evaluated the causal relationship between 402 multi-organ imaging biomarkers and 88 clinical outcomes through bidirectional MR. To circumvent the issue of sample overlap[98], which can bias the causal effect and has been overlooked in many current MR-based studies, we utilized a two-sample MR design and sourced our imaging and clinical data from different large-scale cohorts. The interconnected nature of our organ systems means that diseases often affect more than one part of the human body. The brain and heart are particularly critical, with the brain controlling a variety of

functions, including reactions, emotions, vision, memory, and cognition[99,100], while the heart acts as the body's engine, pumping oxygen and nutrientrich blood to other organs. Dysfunctions in various organs can potentially have detrimental effects on the brain and heart, and vice versa. Besides connections to the brain and heart, we also uncovered many other causal relationships across different organs. A visualization of the interactions across different organ systems can be found in Figure 1B. We will delve into these specific findings in more detail below.

Intra-brain causal connections.

Alternations in brain structure and function were found to be closely linked with brain disorders, with some of these relationships appearing to be bidirectional. We consistently identified causal connections between brain imaging biomarkers and a variety of psychiatric disorders or neurological diseases, such as Alzheimer's disease, dementia, mood disorder, and sleep apnea. For example, Alzheimer's disease and dementia exhibited bidirectional causal relationships with fMRI traits and DTI parameters. Prior studies have consistently reported that resting fMRI connectivity patterns are disrupted in patients with Alzheimer's disease[101,102], particularly in brain regions involved in memory and cognitive function[103,104].

Brain-heart causal connections.

Despite the increasing number of association studies investigating the brain-heart interaction[39,105], causal genetic links within these systems remain largely uncharted. In our research, we identified causal connections from several heart-related diseases such as hypertension, hypertensive diseases, heart failure, and peripheral artery disease, to DTI parameters in white matter tracts. These tracts include the SCR, ALIC, BCC, GCC, the splenium of corpus callosum, and the retrolenticular part of the internal capsule (RLIC). Additionally, these diseases were also linked to regional brain volumes, such as grey matter and left amygdala. Hypertension can lead to damage in the brain's blood vessels[106], which may, in turn, cause a reduction in the volume of grey matter in certain brain regions[107]. This could potentially result in cognitive impairment and an increased risk of developing dementia. Hence, effective management of hypertension through lifestyle adjustments and medication could help mitigate these adverse effects on the brain.

Conversely, we found that alterations in brain structure, such as deformations in the left ventral DC and left basal forebrain, contributed to heart-related diseases like hypertension. Changes in the left superior temporal region were also linked to heart failure. These associations could be attributed to the brain's essential function in regulating blood pressure through a complex network involving multiple regions and pathways[108,109].

Bidirectional connections between the brain and abdominal organs.

Brain abnormalities were found to influence multiple abdominal organs as well as the skeletal system. For example, Alzheimer's disease and dementia were observed causally influencing percent liver fat. Additionally, neurological diseases (defined by FinnGen[27]) exhibited a positive causal effect on lung volume. This could be attributed to the fact that neurological diseases, such as multiple sclerosis, Parkinson's disease, amyotrophic lateral sclerosis, and Huntington's disease, can induce respiratory muscle weakness[110,111]. This weakness could subsequently influence lung volume and functionality. We also found that sleep apnoea may cause an increase in spleen and kidney volume. This could be due to the heightened workload on the spleen to filter blood and remove damaged red blood cells. Additionally, the low oxygen levels associated with sleep apnea can lead to an increase in the number of red blood cells in the body, which could contribute to splenomegaly and a change in kidney volume. Furthermore, sleep apnea was observed to be causally associated with an increase in pancreas iron content. This could potentially be due to the decreased oxygen levels that accompany sleep apnea, resulting in an increase in iron absorption within the body. Excess iron in the pancreas can lead to oxidative stress and inflammation[112,113], which can contribute to the development of pancreatic damage and dysfunction[114-116]. In addition to the previously mentioned neurological diseases, our study revealed that mental and behavioral disorders related to alcohol use can cause an increase in liver fat percentage. It is well documented that individual suffering from alcohol use disorder are more prone to develop alcoholic fatty liver disease[117]. Beyond brain-related diseases, alternations in brain structure could also contribute to a heightened risk of diseases in other organs. For example, changes in the right postcentral gyrus were causally linked to COPD. Some studies suggest that chronic

stress and anxiety, which are associated with changes in brain structure, may contribute to the development or exacerbation of respiratory conditions such as COPD[118,119].

Conversely, brain imaging biomarkers or disorders were causally affected by various diseases of other organs or systems. A high percentage of liver fat led to a reduced risk of Alzheimer's disease and dementia. Past studies[120,121] have reported associations between the two and our results aligned with the most recent study[122]. Further research is necessary to elucidate the underlying pathophysiological mechanism. Brain imaging biomarkers were impacted by diseases across multiple organs, although some may affect the brain indirectly, perhaps via the mediating effects of anxiety and depression. For instance, diseases of the genitourinary system (such as ovarian cyst and menorrhagia) causally influenced brain structural features. Ovarian cysts can cause hormonal imbalances due to the hormones they produce[123]. These hormonal shifts can prompt a variety of symptoms, including mood swings, anxiety, and depression[124], which can impact brain function and emotional regulation. Diseases of the eye and adnexa (conjunctivitis) demonstrated genetic causal effects on functional connectivity traits. Conjunctivitis can result from viral or bacterial infections, potentially leading to systemic inflammation in the body[125]. Such systemic inflammation has been linked to changes in brain function and structure, and may influence brain fMRI traits[126,127].

Moreover, asthma influenced regional brain volumes. A common mechanism through which asthma affects the brain is via the emotional and psychological stress associated with managing a chronic illness. Anxiety, stress, and depression, which are often experienced by individuals with asthma, can result in alterations to brain structure. Prior studies have demonstrated that individuals with asthma may have diminished cognitive function, including impaired memory and attention, as well as changes in brain activity patterns during cognitive tasks[128,129]. Notably, autoimmune diseases (as defined by FinnGen[27]) impacted brain imaging biomarkers, such as DTI parameters of the RLIC and SCR. Multiple sclerosis, an autoimmune disease affecting the central nervous system, can cause damage to the myelin sheath that surrounds axons and can occur in various brain regions[130,131], including the internal capsule. This damage can disrupt neural connections passing through the anterior limb, leading to symptoms like weakness, spasticity, and difficulty with balance and coordination. In rare autoimmune diseases, such as

neuromyelitis optica[132] and autoimmune encephalitis, inflammation, and damage can occur in the brain. The resulting neurological symptoms can vary based on the severity and location of the damage[133,134]. Additionally, autoimmune diseases causing systemic inflammation, such as rheumatoid arthritis and lupus, could potentially affect the brain[135] and white matter tracts[136,137]. Chronic inflammation can lead to changes in the microstructure of white matter tracts, resulting in alterations in neural connectivity and function[138,139].

Intra-heart causal connections.

Bidirectional causal relationships were observed between heart-related diseases and CMR traits. Hypertension and hypertensive diseases were found to causally influence several CMR traits across different heart chambers and aorta regions. Conversely, alternations in CMR traits were suggested to potentially result in heart diseases. These findings corroborate with existing clinical evidence. For example, hypertension can lead to enlargement of the LA, a condition known as left atrial hypertrophy[140,141]. This enlargement can result in various complications, including atrial fibrillation, heart failure, and stroke[142]. In the case of atrial fibrillation, the electrical signals that regulate the heartbeat become erratic, causing an irregular and often repaid heartbeat. Over time, this persistent irregularity can further enlarge and weaken[143].

Bidirectional connections between the heart and abdominal organs.

Heart diseases were found to be causally linked with various multi-organ imaging biomarkers. For instance, heart failure was observed to result in an increase in spleen volume. When the heart is unable to pump blood effectively, it can cause a rise in pressure from the veins leading to the spleen. This increased pressure can cause the spleen to enlarge, a condition known as splenomegaly[144]. In addition, the congestion of blood in the liver, which can occur with heart failure, can also contribute to splenomegaly. Conversely, a larger spleen volume can lead to heart failure. An enlarged spleen can intensify the workload on the heart, leading to further deterioration of heart failure symptoms.

The pancreas was also identified to have a causal effect on the heart. For example, excess pancreas fat was associated with a higher risk of developing deep vein thrombosis of lower extremities and pulmonary embolism. Pancreatic steatosis, a condition where fat accumulates in the pancreas, is linked with several metabolic abnormalities, including insulin resistance and inflammation, which can contribute to the development of cardiovascular diseases[145,146]. The proinflammatory and procoagulant effects of excess pancreatic fat could potentially contribute to an increased risk of deep vein thrombosis.

The heart and lungs are intricately connected, working in conjunction as part of the cardiovascular system. The lungs are responsible for inhaling oxygen from the air and transferring it into the bloodstream, while the heart pumps the oxygen-rich blood throughout the body, nourishing cells and tissues. We identified strong evidence of causal links between COPD and CMR traits of DAo. A hallmark of emphysema is the degradation of elastic fibers via proteolysis[147], which can potentially cause enlargement of the thoracic aorta.

The spleen, as the body's largest immune organ, has been found to be closely related to diseases marked as autoimmune origin. Our study uncovered robust evidence of a genetic causal relationship between spleen volume and autoimmune diseases, as defined by FinnGen[27], including conditions like rheumatoid arthritis, systemic lupus erythematosus, and systemic sclerosis. There are documented instances where autoimmune diseases affect the spleen. For instance, conditions such as lupus or rheumatoid arthritis can result in splenomegaly, a condition that is often triggered by inflammation or the accumulation of abnormal immune cells within the spleen[148,149].

Skeleton DXA traits.

We also found genetic causal connections between DXA-derived skeleton traits and multiple organ diseases. Skeleton traits were shown to be causally affected by diseases of the nervous system, rheumatic disease, and disorders of the nerve, nerve root and plexus. Heart diseases can also influence the skeletal system by influencing bone health. It has been observed that individuals with heart disease, especially those suffering from heart failure, have an increased risk of osteoporosis and bone fractures[149,150]. This can be attributed to various factors. For example, some medications used to treat heart diseases,

such as diuretics and steroids, can increase the risk of osteoporosis[151]. Additionally, individuals with heart disease may experience reduced mobility and physical activity, leading to decreased bone density and strength[152]. Conversely, skeleton problems could contribute to numerous organ diseases, with heart conditions being the most prevalent in our analysis. A longer torso may lead to an increased risk of coronary heart disease. We also observed that a higher average tibia length was causally linked to a lower risk of hypertension, a finding that aligns with previous clinical observations[96].

Limitations and conclusions.

Our study does come with several limitations. Firstly, our collection of GWAS summary statistics was sourced from publicly available databases. Thus, we could not evaluate the impact of unobserved confounders, such as population stratification, on our results. Secondly, a common limitation that most existing MR methods share is that they require several model assumptions. This may result in model misspecifications and issues related to data heterogeneity when integrating data from different data resources[153]. We have systematically applied quality control measures and conducted sensitivity analyses in our study. Future research implementing more advanced MR methods may relax some of these model assumptions[154,155]. Furthermore, MR studies are designed to examine the effects of lifetime exposure factors on outcomes, not interventions within a specified period. As a result, our findings may be interpreted differently than the rigorous results obtained from randomized controlled trials. Therefore, any clinical interventions based on these MR findings should be pursued.

In conclusion, we used two-sample bidirectional MR analyses to comprehensively explore the multi-organ causal connections between 88 clinical outcomes and 402 image-derived phenotypes of various organ systems. Our results revealed robust genetic evidence supporting causal connections within and across multiple organs. This will be instrumental in unraveling complex pathogenic mechanisms and will contribute to the early prediction and prevention of multi-organ diseases from a whole-body perspective.

METHODS

Methods are available in the ***Methods*** section.

Note: One supplementary pdf file and one supplementary table zip file are available.

ACKNOWLEDGEMENTS

The study has been partially supported by funding from the Wharton Dean's Research Fund and Analytics at Wharton, as well as start-up funds from Purdue Statistics Department. This research has been conducted using summary-level data from the UK Biobank study and the FinnGen research project. We would like to thank the individuals who represented themselves in the UK Biobank and FinnGen studies for their participation and the research teams for their efforts in collecting, processing, and disseminating these datasets. We would like to thank the research computing groups at the University of North Carolina at Chapel Hill, Purdue University, and the Wharton School of the University of Pennsylvania for providing computational resources and support that have contributed to these research results.

AUTHOR CONTRIBUTIONS

J.S. and B.Z. designed the study. J.S., R.Z., C.C., B.L., Z. F., X.Y., Y.Y, X.W., and Y.L. analyzed the data. B.X., T.L., and H.Z. provided feedback on the results. J.S. and B.Z. wrote the manuscript with feedback from all authors.

CORRESPONDENCE AND REQUESTS FOR MATERIALS should be addressed to H.Z. and B.Z.

COMPETING FINANCIAL INTERESTS

The authors declare no competing financial interests.

REFERENCES

1. Buckner, R.L.*, et al.* Molecular, structural, and functional characterization of Alzheimer's disease: evidence for a relationship between default activity, amyloid, and memory. *Journal of neuroscience* **25**, 7709-7717 (2005).
2. Pennell, D.J.*, et al.* Clinical indications for cardiovascular magnetic resonance (CMR): Consensus Panel report. *European heart journal* **25**, 1940-1965 (2004).

3. Kun, E.*, et al.* The genetic architecture of the human skeletal form. *bioRxiv*, 2023.2001. 2003.521284 (2023).
4. Petersen, S.E.*, et al.* UK Biobank's cardiovascular magnetic resonance protocol. *Journal of cardiovascular magnetic resonance* **18**, 1-7 (2015).
5. Littlejohns, T.J., Sudlow, C., Allen, N.E. & Collins, R. UK Biobank: opportunities for cardiovascular research. *European heart journal* **40**, 1158-1166 (2019).
6. Miller, K.L.*, et al.* Multimodal population brain imaging in the UK Biobank prospective epidemiological study. *Nature Neuroscience* **19**, 1523-1536 (2016).
7. Thompson, P.M.*, et al.* ENIGMA and global neuroscience: A decade of large-scale studies of the brain in health and disease across more than 40 countries. *Translational psychiatry* **10**, 1-28 (2020).
8. Liu, Y.*, et al.* Genetic architecture of 11 organ traits derived from abdominal MRI using deep learning. *Elife* **10**, e65554 (2021).
9. Smith, S.M. & Nichols, T.E. Statistical challenges in "big data" human neuroimaging. *Neuron* **97**, 263-268 (2018).
10. Tian, Y.E.*, et al.* Heterogeneous aging across multiple organ systems and prediction of chronic disease and mortality. *Nature Medicine*, 1-11 (2023).
11. Taschler, B., Smith, S.M. & Nichols, T.E. Causal inference on neuroimaging data with Mendelian randomisation. *NeuroImage*, 119385 (2022).
12. Sanderson, E.*, et al.* Mendelian randomization. *Nature Reviews Methods Primers* **2**, 1-21 (2022).
13. Pingault, J.-B.*, et al.* Using genetic data to strengthen causal inference in observational research. *Nature Reviews Genetics* **19**, 566-580 (2018).
14. Aung, N.*, et al.* Genome-wide analysis of left ventricular image-derived phenotypes identifies fourteen loci associated with cardiac morphogenesis and heart failure development. *Circulation* **140**, 1318-1330 (2019).
15. Córdova-Palomera, A.*, et al.* Cardiac Imaging of Aortic Valve Area From 34 287 UK Biobank Participants Reveals Novel Genetic Associations and Shared Genetic Comorbidity With Multiple Disease Phenotypes. *Circulation: Genomic and Precision Medicine* **13**, e003014 (2020).
16. Meyer, H.V.*, et al.* Genetic and functional insights into the fractal structure of the heart. *Nature* **584**, 589-594 (2020).

17. Pirruccello, J.P.*, et al.* Analysis of cardiac magnetic resonance imaging in 36,000 individuals yields genetic insights into dilated cardiomyopathy. *Nature communications* **11**, 1-10 (2020).
18. Pirruccello, J.P.*, et al.* Genetic Analysis of Right Heart Structure and Function in 40,000 People. *bioRxiv* (2021).
19. Thanaj, M.*, et al.* Genetic and environmental determinants of diastolic heart function. *medRxiv* (2021).
20. Elliott, L.T.*, et al.* Genome-wide association studies of brain imaging phenotypes in UK Biobank. *Nature* **562**, 210-216 (2018).
21. Zhao, B.*, et al.* Genome-wide association analysis of 19,629 individuals identifies variants influencing regional brain volumes and refines their genetic co-architecture with cognitive and mental health traits. *Nature genetics* **51**, 1637-1644 (2019).
22. Smith, S.M.*, et al.* An expanded set of genome-wide association studies of brain imaging phenotypes in UK Biobank. *Nature neuroscience* **24**, 737-745 (2021).
23. Zhao, B.*, et al.* Common genetic variation influencing human white matter microstructure. *Science* **372**, eabf3736 (2021).
24. Grasby, K.L.*, et al.* The genetic architecture of the human cerebral cortex. *Science* **367**, eaay6690 (2020).
25. Zhao, B.*, et al.* Genetic influences on the intrinsic and extrinsic functional organizations of the cerebral cortex. *medRxiv*, 2021.2007. 2027.21261187 (2021).
26. Watanabe, K.*, et al.* A global overview of pleiotropy and genetic architecture in complex traits. *Nature genetics* **51**, 1339-1348 (2019).
27. Kurki, M.I.*, et al.* FinnGen: Unique genetic insights from combining isolated population and national health register data. *medRxiv* (2022).
28. Flynn, B.I.*, et al.* Deep learning based phenotyping of medical images improves power for gene discovery of complex disease. *medRxiv*, 2023.2003. 2007.23286909 (2023).
29. Kun, E.*, et al.* The genetic architecture of the human skeletal form. *bioRxiv* (2023).

30. Guo, J.*, et al.* Mendelian randomization analyses support causal relationships between brain imaging-derived phenotypes and risk of psychiatric disorders. *Nature Neuroscience* **25**, 1519-1527 (2022).
31. Chen, X.*, et al.* Kidney damage causally affects the brain cortical structure: a Mendelian randomization study. *EBioMedicine* **72**, 103592 (2021).
32. Williams, J.A.*, et al.* Inflammation and brain structure in schizophrenia and other neuropsychiatric disorders: a Mendelian randomization study. *JAMA psychiatry* **79**, 498-507 (2022).
33. Topiwala, A.*, et al.* Associations between moderate alcohol consumption, brain iron, and cognition in UK Biobank participants: observational and mendelian randomization analyses. *PLoS medicine* **19**, e1004039 (2022).
34. Holmes, M.V.*, et al.* Mendelian randomization of blood lipids for coronary heart disease. *European heart journal* **36**, 539-550 (2015).
35. Lamina, C. & Kronenberg, F. Estimation of the required lipoprotein (a)-lowering therapeutic effect size for reduction in coronary heart disease outcomes: a Mendelian randomization analysis. *JAMA cardiology* **4**, 575-579 (2019).
36. Sudlow, C.*, et al.* UK biobank: an open access resource for identifying the causes of a wide range of complex diseases of middle and old age. *PLoS medicine* **12**, e1001779 (2015).
37. Bijsterbosch, J.*, et al.* Investigations into within-and between-subject resting-state amplitude variations. *Neuroimage* **159**, 57-69 (2017).
38. Bai, W.*, et al.* A population-based phenome-wide association study of cardiac and aortic structure and function. *Nature Medicine* **26**, 1654-1662 (2020).
39. Zhao, B.*, et al.* Heart-brain connections: phenotypic and genetic insights from magnetic resonance images. *Science*, just-accepted (2023).
40. Bowden, J.*, et al.* A framework for the investigation of pleiotropy in two-sample summary data Mendelian randomization. *Statistics in medicine* **36**, 1783-1802 (2017).
41. Burgess, S., Butterworth, A. & Thompson, S.G. Mendelian randomization analysis with multiple genetic variants using summarized data. *Genetic epidemiology* **37**, 658-665 (2013).

42. Bowden, J.*, et al.* Improving the accuracy of two-sample summary-data Mendelian randomization: moving beyond the NOME assumption. *Int J Epidemiol* **48**, 728-742 (2019).
43. Bowden, J., Davey Smith, G. & Burgess, S. Mendelian randomization with invalid instruments: effect estimation and bias detection through Egger regression. *International journal of epidemiology* **44**, 512-525 (2015).
44. Hartwig, F.P., Davey Smith, G. & Bowden, J. Robust inference in summary data Mendelian randomization via the zero modal pleiotropy assumption. *International journal of epidemiology* **46**, 1985-1998 (2017).
45. Bowden, J., Davey Smith, G., Haycock, P.C. & Burgess, S. Consistent estimation in Mendelian randomization with some invalid instruments using a weighted median estimator. *Genetic epidemiology* **40**, 304-314 (2016).
46. Ye, T., Shao, J. & Kang, H. Debiased inverse-variance weighted estimator in two-sample summary-data Mendelian randomization. *The Annals of statistics* **49**, 2079-2100 (2021).
47. Zhao, Q., Wang, J., Hemani, G., Bowden, J. & Small, D.S. Statistical inference in two-sample summary-data Mendelian randomization using robust adjusted profile score. *The Annals of Statistics* **48**, 1742-1769 (2020).
48. Wang, J.*, et al.* Causal inference for heritable phenotypic risk factors using heterogeneous genetic instruments. *PLoS genetics* **17**, e1009575 (2021).
49. Oishi, K., Mielke, M.M., Albert, M., Lyketsos, C.G. & Mori, S. DTI analyses and clinical applications in Alzheimer's disease. *J Alzheimers Dis* **26 Suppl 3**, 287-296 (2011).
50. Yin, R.-H.*, et al.* Multimodal voxel-based meta-analysis of white matter abnormalities in Alzheimer's disease. *Journal of Alzheimer's Disease* **47**, 495-507 (2015).
51. Li, R.*, et al.* Attention-related networks in Alzheimer's disease: A resting functional MRI study. *Human brain mapping* **33**, 1076-1088 (2012).
52. Stratos, C., Stefanadis, C., Kallikazaros, I., Boudoulas, H. & Toutouzas, P. Ascending aorta distensibility abnormalities in hypertensive patients and response to nifedipine administration. *The American journal of medicine* **93**, 505-512 (1992).

53. Asmar, R.*, et al.* Aortic distensibility in normotensive, untreated and treated hypertensive patients. *Blood pressure* **4**, 48-54 (1995).
54. Nabati, M., Namazi, S.S., Yazdani, J. & Sharif Nia, H. Relation between aortic stiffness index and distensibility with age in hypertensive patients. *International journal of general medicine*, 297-303 (2020).
55. Lembo, M.*, et al.* Advanced imaging tools for evaluating cardiac morphological and functional impairment in hypertensive disease. *Journal of Hypertension* **40**, 4-14 (2022).
56. Di Palo, K.E. & Barone, N.J. Hypertension and heart failure: prevention, targets, and treatment. *Heart failure clinics* **16**, 99-106 (2020).
57. Gopinathannair, R.*, et al.* Managing atrial fibrillation in patients with heart failure and reduced ejection fraction: a scientific statement from the American Heart Association. *Circulation: Arrhythmia and Electrophysiology* **14**, e000078 (2021).
58. Packer, M. Do most patients with obesity or type 2 diabetes, and atrial fibrillation, also have undiagnosed heart failure? A critical conceptual framework for understanding mechanisms and improving diagnosis and treatment. *European journal of heart failure* **22**, 214-227 (2020).
59. Fujikura, K.*, et al.* Aortic enlargement in chronic obstructive pulmonary disease (COPD) and emphysema: The Multi-Ethnic Study of Atherosclerosis (MESA) COPD study. *Int J Cardiol* **331**, 214-220 (2021).
60. Maclay, J.D.*, et al.* Systemic elastin degradation in chronic obstructive pulmonary disease. *Thorax* **67**, 606-612 (2012).
61. Berman, M.N., Tupper, C. & Bhardwaj, A. Physiology, Left Ventricular Function. (2019).
62. Kim, D.-Y. & Camilleri, M. Serotonin: a mediator of the brain–gut connection. *Official journal of the American College of Gastroenterology| ACG* **95**, 2698-2709 (2000).
63. Jones, M., Dilley, J., Drossman, D. & Crowell, M. Brain–gut connections in functional GI disorders: anatomic and physiologic relationships. *Neurogastroenterology & Motility* **18**, 91-103 (2006).
64. Keefer, L.*, et al.* A Rome working team report on brain-gut behavior therapies for disorders of gut-brain interaction. *Gastroenterology* **162**, 300-315 (2022).

65. Xie, Z., Tong, S., Chu, X., Feng, T. & Geng, M. Chronic kidney disease and cognitive impairment: The kidney-brain axis. *Kidney Diseases* **8**, 275-285 (2022).
66. de Donato, A., Buonincontri, V., Borriello, G., Martinelli, G. & Mone, P. The dopamine system: insights between kidney and brain. *Kidney and Blood Pressure Research* **47**, 493-505 (2022).
67. McCracken, C*., et al.* Multi-organ imaging demonstrates the heart-brain-liver axis in UK Biobank participants. *Nature Communications* **13**, 7839 (2022).
68. Voulgaris, A., Marrone, O., Bonsignore, M.R. & Steiropoulos, P. Chronic kidney disease in patients with obstructive sleep apnea. A narrative review. *Sleep Medicine Reviews* **47**, 74-89 (2019).
69. Sim, J.J., Rasgon, S.A. & Derose, S.F. Managing sleep apnoea in kidney diseases. *Nephrology* **15**, 146-152 (2010).
70. O'Reilly, R.A. Splenomegaly in 2,505 patients in a large university medical center from 1913 to 1995. 1913 to 1962: 2,056 patients. *Western journal of medicine* **169**, 78 (1998).
71. Vinchi, F*., et al.* Atherosclerosis is aggravated by iron overload and ameliorated by dietary and pharmacological iron restriction. *European heart journal* **41**, 2681-2695 (2020).
72. Kempf, T. & Wollert, K.C. Iron and atherosclerosis: too much of a good thing can be bad. *European Heart Journal* (2020).
73. Balint, G.P. & Balint, P.V. Felty's syndrome. *Best practice & research clinical rheumatology* **18**, 631-645 (2004).
74. Blendis, L., Ansell, I., Jones, K.L., Hamilton, E. & Williams, R. Liver in Felty's syndrome. *Br Med J* **1**, 131-135 (1970).
75. Kataria, Y.P. & Whitcomb, M.E. Splenomegaly in sarcoidosis. *Archives of Internal Medicine* **140**, 35-37 (1980).
76. Candia, L., Marquez, J. & Espinoza, L.R. Autoimmune hepatitis and pregnancy: a rheumatologist's dilemma. in *Seminars in arthritis and rheumatism*, Vol. 35 49-56 (Elsevier, 2005).
77. Wang, Z*., et al.* Iron drives T helper cell pathogenicity by promoting RNA-binding protein PCBP1-mediated proinflammatory cytokine production. *Immunity* **49**, 80-92. e87 (2018).

78. Erie, J.C.*, et al.* Heavy metal concentrations in human eyes. *American journal of ophthalmology* **139**, 888-893 (2005).
79. Honka, H.*, et al.* The effects of bariatric surgery on pancreatic lipid metabolism and blood flow. *The Journal of Clinical Endocrinology & Metabolism* **100**, 2015-2023 (2015).
80. Huang, J.-A., Lin, C.-H., Chang, Y.-T., Lee, C.-T. & Wu, M.-J. Nephrotic syndrome is associated with increased risk of ischemic stroke. *Journal of Stroke and Cerebrovascular Diseases* **28**, 104322 (2019).
81. Gigante, A.*, et al.* Nephrotic syndrome and stroke. *International Journal of Immunopathology and Pharmacology* **26**, 769-772 (2013).
82. Roy, C.*, et al.* Ischemic stroke of possible embolic etiology associated with nephrotic syndrome. *Kidney International Reports* **2**, 988-994 (2017).
83. Cheon, S.Y. & Song, J. Novel insights into non-alcoholic fatty liver disease and dementia: insulin resistance, hyperammonemia, gut dysbiosis, vascular impairment, and inflammation. *Cell & Bioscience* **12**, 1-14 (2022).
84. Rodrigo, R.*, et al.* Hyperammonemia induces neuroinflammation that contributes to cognitive impairment in rats with hepatic encephalopathy. *Gastroenterology* **139**, 675-684 (2010).
85. Rose, C.F.*, et al.* Hepatic encephalopathy: Novel insights into classification, pathophysiology and therapy. *Journal of hepatology* **73**, 1526-1547 (2020).
86. Kong, S.H., Park, Y.J., Lee, J.-Y., Cho, N.H. & Moon, M.K. Insulin resistance is associated with cognitive decline among older Koreans with normal baseline cognitive function: a prospective community-based cohort study. *Scientific reports* **8**, 650 (2018).
87. Hobson-Webb, L.D., Massey, J.M., Juel, V.C. & Sanders, D.B. The ultrasonographic wrist-to-forearm median nerve area ratio in carpal tunnel syndrome. *Clinical neurophysiology* **119**, 1353-1357 (2008).
88. Paluch, Ł., Pietruski, P., Walecki, J. & Noszczyk, B.H. Wrist to forearm ratio as a median nerve shear wave elastography test in carpal tunnel syndrome diagnosis. *Journal of Plastic, Reconstructive & Aesthetic Surgery* **71**, 1146-1152 (2018).

89. Gotsopoulos, H., Chen, C., Qian, J. & Cistulli, P.A. Oral appliance therapy improves symptoms in obstructive sleep apnea: a randomized, controlled trial. *American journal of respiratory and critical care medicine* **166**, 743-748 (2002).
90. Araie, T., Okuno, K., Minagi, H.O. & Sakai, T. Dental and skeletal changes associated with long-term oral appliance use for obstructive sleep apnea: a systematic review and meta-analysis. *Sleep Medicine Reviews* **41**, 161-172 (2018).
91. Sander, J.E. & Sharp, F.R. Lumbosacral plexus neuritis. *Neurology* **31**, 470-473 (1981).
92. Khamis, S. & Carmeli, E. A new concept for measuring leg length discrepancy. *Journal of orthopaedics* **14**, 276-280 (2017).
93. Raczkowski, J.W., Daniszewska, B. & Zolynski, K. Functional scoliosis caused by leg length discrepancy. *Archives of Medical Science* **6**, 393-398 (2010).
94. Nelson, C.P.*, et al.* Genetically determined height and coronary artery disease. *New England Journal of Medicine* **372**, 1608-1618 (2015).
95. Schmidt, M., Bøtker, H.E., Pedersen, L. & Sørensen, H.T. Adult height and risk of ischemic heart disease, atrial fibrillation, stroke, venous thromboembolism, and premature death: a population based 36-year follow-up study. *European journal of epidemiology* **29**, 111-118 (2014).
96. Yin, F., Spurgeon, H.A., Rakusan, K., Weisfeldt, M.L. & Lakatta, E.G. Use of tibial length to quantify cardiac hypertrophy: application in the aging rat. *American Journal of Physiology-Heart and Circulatory Physiology* **243**, H941-H947 (1982).
97. Walker, V.M., Zheng, J., Gaunt, T.R. & Smith, G.D. Phenotypic Causal Inference Using Genome-Wide Association Study Data: Mendelian Randomization and Beyond. *Annu Rev Biomed Data Sci* **5**, 1-17 (2022).
98. Burgess, S., Davies, N.M. & Thompson, S.G. Bias due to participant overlap in two-sample Mendelian randomization. *Genetic epidemiology* **40**, 597-608 (2016).
99. Berridge, K.C. & Kringelbach, M.L. Pleasure systems in the brain. *Neuron* **86**, 646-664 (2015).
100. Bressler, S.L. & Menon, V. Large-scale brain networks in cognition: emerging methods and principles. *Trends Cogn Sci* **14**, 277-290 (2010).

101. Wang, K.*, et al.* Altered functional connectivity in early Alzheimer's disease: A resting-state fMRI study. *Human brain mapping* **28**, 967-978 (2007).
102. Sorg, C.*, et al.* Selective changes of resting-state networks in individuals at risk for Alzheimer's disease. *Proceedings of the National Academy of Sciences* **104**, 18760-18765 (2007).
103. Ranasinghe, K.G.*, et al.* Regional functional connectivity predicts distinct cognitive impairments in Alzheimer's disease spectrum. *NeuroImage: Clinical* **5**, 385-395 (2014).
104. Pini, L.*, et al.* A low-dimensional cognitive-network space in Alzheimer's disease and frontotemporal dementia. *Alzheimer's Research & Therapy* **14**, 199 (2022).
105. Liu, W.*, et al.* Brain–heart communication in health and diseases. *Brain Research Bulletin* (2022).
106. Walker, K.A., Power, M.C. & Gottesman, R.F. Defining the relationship between hypertension, cognitive decline, and dementia: a review. *Current hypertension reports* **19**, 1-16 (2017).
107. Zhang, H.*, et al.* Reduced regional gray matter volume in patients with chronic obstructive pulmonary disease: a voxel-based morphometry study. *American Journal of Neuroradiology* **34**, 334-339 (2013).
108. do Carmo, J.M.*, et al.* Role of the brain melanocortins in blood pressure regulation. *Biochimica et Biophysica Acta (BBA)-Molecular Basis of Disease* **1863**, 2508-2514 (2017).
109. Goriely, A.*, et al.* Mechanics of the brain: perspectives, challenges, and opportunities. *Biomechanics and modeling in mechanobiology* **14**, 931-965 (2015).
110. Polkey, M.I., Lyall, R.A., Moxham, J. & Leigh, P.N. Respiratory aspects of neurological disease. *Journal of Neurology, Neurosurgery & Psychiatry* **66**, 5-15 (1999).
111. Pollock, R.D., Rafferty, G.F., Moxham, J. & Kalra, L. Respiratory muscle strength and training in stroke and neurology: a systematic review. *International Journal of Stroke* **8**, 124-130 (2013).

112. Tian, C., Zhao, J., Xiong, Q., Yu, H. & Du, H. Secondary iron overload induces chronic pancreatitis and ferroptosis of acinar cells in mice. *International Journal of Molecular Medicine* **51**, 1-13 (2023).
113. Galaris, D., Barbouti, A. & Pantopoulos, K. Iron homeostasis and oxidative stress: An intimate relationship. *Biochimica et Biophysica Acta (BBA)-Molecular Cell Research* **1866**, 118535 (2019).
114. Robles, L., Vaziri, N.D. & Ichii, H. Role of oxidative stress in the pathogenesis of pancreatitis: effect of antioxidant therapy. *Pancreatic disorders & therapy* **3**, 112 (2013).
115. Armstrong, J.*, et al.* Oxidative stress in acute pancreatitis: lost in translation? *Free radical research* **47**, 917-933 (2013).
116. Pérez, S., Pereda, J., Sabater, L. & Sastre, J. Redox signaling in acute pancreatitis. *Redox biology* **5**, 1-14 (2015).
117. Kushner, T. & Cafardi, J. Chronic liver disease and COVID-19: alcohol use disorder/alcohol-associated liver disease, nonalcoholic fatty liver disease/nonalcoholic steatohepatitis, autoimmune liver disease, and compensated cirrhosis. *Clinical Liver Disease* **15**, 195 (2020).
118. Grant, I., Heaton, R.K., McSweeney, A.J., Adams, K.M. & Timms, R.M. Brain dysfunction in COPD. *Chest* **77**, 308-309 (1980).
119. Spilling, C.A.*, et al.* Factors affecting brain structure in smoking-related diseases: Chronic Obstructive Pulmonary Disease (COPD) and coronary artery disease. *PLoS One* **16**, e0259375 (2021).
120. Kim, G.A.*, et al.* Association between non-alcoholic fatty liver disease and the risk of dementia: a nationwide cohort study. *Liver international* **42**, 1027-1036 (2022).
121. Kim, D.-G.*, et al.* Non-alcoholic fatty liver disease induces signs of Alzheimer's disease (AD) in wild-type mice and accelerates pathological signs of AD in an AD model. *Journal of neuroinflammation* **13**, 1-18 (2016).
122. Wang, L., Sang, B. & Zheng, Z. Risk of dementia or cognitive impairment in non-alcoholic fatty liver disease: A systematic review and meta-analysis. *Frontiers in Aging Neuroscience* **14**(2022).
123. Mobeen, S. & Apostol, R. Ovarian cyst. (2020).

124. Padda, J.*, et al.* Depression and its effect on the menstrual cycle. *Cureus* **13**(2021).
125. Azari, A.A. & Barney, N.P. Conjunctivitis: a systematic review of diagnosis and treatment. *Jama* **310**, 1721-1730 (2013).
126. Sankowski, R., Mader, S. & Valdés-Ferrer, S.I. Systemic inflammation and the brain: novel roles of genetic, molecular, and environmental cues as drivers of neurodegeneration. *Frontiers in cellular neuroscience* **9**, 28 (2015).
127. Elwood, E., Lim, Z., Naveed, H. & Galea, I. The effect of systemic inflammation on human brain barrier function. *Brain, behavior, and immunity* **62**, 35-40 (2017).
128. Rhyou, H.-I. & Nam, Y.-H. Association between cognitive function and asthma in adults. *Annals of Allergy, Asthma & Immunology* **126**, 69-74 (2021).
129. Ray, M., Sano, M., Wisnivesky, J.P., Wolf, M.S. & Federman, A.D. Asthma control and cognitive function in a cohort of elderly adults. *Journal of the American Geriatrics Society* **63**, 684-691 (2015).
130. Alvarez, J.I., Cayrol, R. & Prat, A. Disruption of central nervous system barriers in multiple sclerosis. *Biochimica et Biophysica Acta (BBA)-Molecular Basis of Disease* **1812**, 252-264 (2011).
131. Krupp, L.B.*, et al.* International Pediatric Multiple Sclerosis Study Group criteria for pediatric multiple sclerosis and immune-mediated central nervous system demyelinating disorders: revisions to the 2007 definitions. *Multiple Sclerosis Journal* **19**, 1261-1267 (2013).
132. Huda, S.*, et al.* Neuromyelitis optica spectrum disorders. *Clinical Medicine* **19**, 169 (2019).
133. Kim, W., Kim, S.-H., Huh, S.-Y. & Kim, H.J. Brain abnormalities in neuromyelitis optica spectrum disorder. *Multiple sclerosis international* **2012**(2012).
134. Lancaster, E. The diagnosis and treatment of autoimmune encephalitis. *Journal of Clinical Neurology* **12**, 1-13 (2016).
135. Wartolowska, K.*, et al.* Structural changes of the brain in rheumatoid arthritis. *Arthritis & Rheumatism* **64**, 371-379 (2012).
136. Kozora, E. & Filley, C.M. Cognitive dysfunction and white matter abnormalities in systemic lupus erythematosus. *Journal of the International Neuropsychological Society* **17**, 385-392 (2011).

137. Appenzeller, S*., et al.* Longitudinal analysis of gray and white matter loss in patients with systemic lupus erythematosus. *Neuroimage* **34**, 694-701 (2007).
138. Rosenberg, G.A. Inflammation and white matter damage in vascular cognitive impairment. *Stroke* **40**, S20-S23 (2009).
139. Raj, D*., et al.* Increased white matter inflammation in aging-and Alzheimer's disease brain. *Frontiers in molecular neuroscience* **10**, 206 (2017).
140. Gerdts, E*., et al.* Correlates of left atrial size in hypertensive patients with left ventricular hypertrophy: the Losartan Intervention For Endpoint Reduction in Hypertension (LIFE) Study. *Hypertension* **39**, 739-743 (2002).
141. Eshoo, S., Ross, D.L. & Thomas, L. Impact of mild hypertension on left atrial size and function. *Circulation: Cardiovascular Imaging* **2**, 93-99 (2009).
142. Sanfilippo, A.J*., et al.* Atrial enlargement as a consequence of atrial fibrillation. A prospective echocardiographic study. *Circulation* **82**, 792-797 (1990).
143. van de Vegte, Y.J., Siland, J.E., Rienstra, M. & van der Harst, P. Atrial fibrillation and left atrial size and function: a Mendelian randomization study. *Scientific reports* **11**, 8431 (2021).
144. Hiraiwa, H*., et al.* Clinical significance of spleen size in patients with heart failure. *European Heart Journal* **42**, ehab724. 0756 (2021).
145. Ormazabal, V*., et al.* Association between insulin resistance and the development of cardiovascular disease. *Cardiovascular diabetology* **17**, 1-14 (2018).
146. Shah, A., Mehta, N. & Reilly, M.P. Adipose inflammation, insulin resistance, and cardiovascular disease. *Journal of Parenteral and Enteral Nutrition* **32**, 638-644 (2008).
147. Thurlbeck, W.M. & Müller, N. Emphysema: definition, imaging, and quantification. *AJR. American journal of roentgenology* **163**, 1017-1025 (1994).
148. Fernández-García, V., González-Ramos, S., Martín-Sanz, P., Castrillo, A. & Boscá, L. Contribution of extramedullary hematopoiesis to atherosclerosis. The spleen as a neglected hub of inflammatory cells. *Frontiers in Immunology* **11**, 586527 (2020).
149. Suttorp, M. & Classen, C.F. Splenomegaly in children and adolescents. *Frontiers in pediatrics*, 693 (2021).

150. Lampropoulos, C.E., Papaioannou, I. & D'cruz, D.P. Osteoporosis—a risk factor for cardiovascular disease? *Nature Reviews Rheumatology* **8**, 587-598 (2012).
151. Gaines, J.M.*, et al.* Older men's knowledge of osteoporosis and the prevalence of risk factors. *Journal of Clinical Densitometry* **13**, 204-209 (2010).
152. Whalen, R., Carter, D. & Steele, C. Influence of physical activity on the regulation of bone density. *Journal of biomechanics* **21**, 825-837 (1988).
153. Zhao, Q., Wang, J., Spiller, W., Bowden, J. & Small, D.S. Two-sample instrumental variable analyses using heterogeneous samples. *Statistical Science* **34**, 317-333 (2019).
154. Cui, R.*, et al.* Improving fine-mapping by modeling infinitesimal effects. *bioRxiv*, 2022.2010. 2021.513123 (2022).
155. Xue, H., Shen, X. & Pan, W. Causal Inference in Transcriptome-Wide Association Studies with Invalid Instruments and GWAS Summary Data. *Journal of the American Statistical Association*, 1-27 (2023).
156. Tseng, W.Y., Su, M.Y. & Tseng, Y.H. Introduction to Cardiovascular Magnetic Resonance: Technical Principles and Clinical Applications. *Acta Cardiol Sin* **32**, 129-144 (2016).
157. Pennell, D.J. Cardiovascular magnetic resonance. *Circulation* **121**, 692-705 (2010).
158. Bai, W.*, et al.* Automated cardiovascular magnetic resonance image analysis with fully convolutional networks. *Journal of Cardiovascular Magnetic Resonance* **20**, 1-12 (2018).
159. Bai, W.*, et al.* Recurrent neural networks for aortic image sequence segmentation with sparse annotations. *International conference on medical image computing and computer-assisted intervention*, 586-594 (2018).
160. Miller, K.L.*, et al.* Multimodal population brain imaging in the UK Biobank prospective epidemiological study. *Nat Neurosci* **19**, 1523-1536 (2016).
161. Zhao, B.*, et al.* Heritability of regional brain volumes in large-scale neuroimaging and genetic studies. *Cerebral Cortex* **29**, 2904-2914 (2019).
162. Zhao, B.*, et al.* Large-scale GWAS reveals genetic architecture of brain white matter microstructure and genetic overlap with cognitive and mental health traits (n= 17,706). *Molecular psychiatry* **26**, 3943-3955 (2021).

163. Avants, B.B.*, et al.* A reproducible evaluation of ANTs similarity metric performance in brain image registration. *Neuroimage* **54**, 2033-2044 (2011).
164. Jahanshad, N.*, et al.* Multi-site genetic analysis of diffusion images and voxelwise heritability analysis: A pilot project of the ENIGMA–DTI working group. *Neuroimage* **81**, 455-469 (2013).
165. Kochunov, P.*, et al.* Multi-site study of additive genetic effects on fractional anisotropy of cerebral white matter: comparing meta and megaanalytical approaches for data pooling. *Neuroimage* **95**, 136-150 (2014).
166. Glasser, M.F.*, et al.* A multi-modal parcellation of human cerebral cortex. *Nature* **536**, 171-178 (2016).
167. Ji, J.L.*, et al.* Mapping the human brain's cortical-subcortical functional network organization. *Neuroimage* **185**, 35-57 (2019).
168. Bowden, J.*, et al.* Improving the accuracy of two-sample summary-data Mendelian randomization: moving beyond the NOME assumption. *International journal of epidemiology* **48**, 728-742 (2019).

METHODS

Multi-organ imaging biomarkers.

The imaging data were sourced from the UK Biobank (UKB) study, which enrolled approximately 500,000 individuals aged between 40 and 69 from 2006 to 2010 (https://www.ukbiobank.ac.uk/). These multi-organ imaging data were collected from the ongoing UKB imaging study project (https://www.ukbiobank.ac.uk/explore-your-participation/contribute-further/imaging-study), which aims to collect brain, heart, and abdomen scans from 100,000 participants. Ethical approval for the UKB study was secured from the North West Multicentre Research Ethics Committee (approval number: 11/NW/0382).

Studies of brain and heart diseases usually rely on magnetic resonance imaging (MRI) scans, which are well-established clinical endophenotypes. Cardiovascular magnetic resonance imaging (CMR) is a set of MRI techniques that are designed to assess ventricular function, cardiovascular morphology, myocardial perfusion, and other cardiac functional and structural features[156,157]. They have been frequently used to reveal heart-

related issues clinically. The CMR traits used in the paper were originally generated from the raw short-axis, long-axis, and aortic cine images using the state-of-the-art heart imaging segmentation and feature representation framework[38,158,159]. We divided the generated 82 CMR traits into 6 categories. The first two are aortic sections, namely ascending aorta (AAo) and descending aorta (DAo), which serve as the main 'pipe' in supplying blood to the entire body. The other four are the global measures of 4 cardiac chambers, including the left ventricle (LV), right ventricle (RV), left atrium (LA), and right atrium (RA), which altogether manage the heartbeat and blood flow. There are also some other traits, such as regional phenotypes of the left ventricle myocardial-wall thickness and strain (**Table S1**). The summary-level GWAS data of these 82 CMR traits were obtained from Zhao, et al. [39].

Brain MRI provides detailed information about brain structure and function[160], such as abnormal growth, healthy aging, white matter diseases, structural issues, and functional abnormalities. In this paper, the summary-level GWAS data were collected from recent multi-modal image genetic studies, including regional brain volumes from structural MRI[21,161] (sMRI), diffusion tensor imaging (DTI) parameters from diffusion MRI[23,162] (dMRI), and functional activity (that is, amplitude[37]) and functional connectivity phenotypes from resting functional MRI[25] (resting fMRI). In sMRI, we used ANTs[163] to generate regional brain volumes for cortical and subcortical regions and global brain volume measures. In dMRI, we used the ENIGMA-DTI pipelines[164,165] to generate tract-averaged parameters for fractional anisotropy, mean diffusivity, axial diffusivity, radial diffusivity, and mode of anisotropy in major white matter tracts and across the whole brain. For resting fMRI, we extracted phenotypes from brain parcellation-based analysis. We used the Glasser360 atlas[166], which divided the cerebral cortex into 360 regions in 12 functional networks[167]. We considered 90 network-level resting fMRI phenotypes that evaluated interactions and spontaneous neural activity at rest.

The 11 imaging biomarkers from abdominal MRI were derived by Liu., et al[8] using deep learning methods in terms of volume, fat, and iron in several organs and tissues, such as the liver, spleen, kidney, lung, pancreas, and adipose tissue. Skeleton DXA traits, including all long bone lengths as well as hip and shoulder width, were derived by Kun., et al[3] using

deep learning methods on whole-body dual-energy X-ray absorptiometry (DXA) images. All eight skeleton traits have been controlled for height. The heritability of the above imaging biomarkers can be found in **Supplementary Note**.

FinnGen clinical endpoints.

We used 88 clinical endpoints collected by the FinnGen project, which were selected from the R7 release and with more than 10,000 cases for most of the clinical endpoints (https://www.finngen.fi/en/access_results). As for some important diseases, such as Alzheimer's disease, we set the cutoff of the number of cases to be 6,000. The 88 clinical endpoints covered diseases from various categories, namely, mental and behavioral disorders, diseases of the nervous system, diseases of the eye and adnexa, diseases of the genitourinary system, diseases of the circulatory systems, cardiometabolic endpoints, diseases marked as autoimmune origin, rheuma endpoints, interstitial lung diseases, COPD and related endpoints, as well as some unclassified endpoints. The definitions can be found at https://risteys.finregistry.fi/. The FinnGen data used in our study was obtained from separate cohorts than those supplying imaging biomarkers, which were derived from the UKB study, thus ensuring there was no sample overlap. Detailed information of these 88 clinical variables can be found in **Table S2**.

Mendelian randomization analysis.

We examined the genetic causal relationships between the 402 imaging biomarkers (101 brain regional volume traits, 110 brain DTI parameters, 90 network-level fMRI phenotypes, 82 CMR traits, 11 abdominal traits, and 8 skeleton DXA traits) and 88 clinical endpoints. Prior to conducting the Mendelian randomization (MR) analysis, we conducted standard preprocessing and quality control procedures. First, we selected genetic variants based on a significance threshold of 5×10^{-8} in the exposure GWAS data. To ensure the independence of the genetic variants used in MR, we implemented LD clumping with a window size of 10,000 and an r^2 threshold of 0.01, using the 1000 Genomes European ancestry data as a reference panel. We used the TwoSampleMR package (https://mrcieu.github.io/TwoSampleMR/) for harmonization, which enabled us to accurately align alleles between the selected variants in the exposure and the reported effect on the outcome.

We assessed the performance of 8 MR methods, which included Inverse variance weighted (fixed effect), Inverse variance weighted (multiplicative random effect), MR-Egger, Simple Median, Weighted Median, Weighted Mode, DIVW, GRAPPLE, and MR-RAPS[40,41,43-48,168], where MR Egger was used as the pleiotropy test. To ensure the reliability of our results, we implemented several quality control procedures. We excluded causal estimates that relied on fewer than 6 genetic variants, as a larger number of genetic variants increases the statistical power of MR analysis[46,47]. We retained causal pairs that were significant in at least two out of the eight methods. We also screened for pleiotropy by using the MR-Egger intercept, the most used method for testing the pleiotropy assumption. If a causal estimate failed the MR-Egger intercept test, we required that it have significant results in at least one of the robust MR methods, such as Weighted Median, Weighted Model, MR-RAPS, or GRAPPLE. Out of 488 significant findings, 81 causal estimates failed the MR-Egger intercept test. However, when we interpreted the results, we focused on the ones that passed the MR-Egger intercept test.

Code availability

We made use of publicly available software and tools. Our analysis code will be made freely available at Zenodo.

Data availability

We used summary-level GWAS data in this study, which can be obtained from the FinnGen project (https://www.finngen.fi/en/access_results), BIG-KP (https://bigkp.org/), Heart-KP (https://heartkp.org/), and project-specific resources detailed in Liu., et al[8] and Kun., et al[3]. Our multi-organ MR results can be explored at https://mr4mo.org/.

Figure legends

Fig. 1 Overview of study design and findings.

(**A**). An overview of our multi-organ imaging genetic study, investigating 88 clinical outcomes. We employed diverse imaging biomarkers including multi-modal brain,

cardiac, abdominal, and skeletal DXA imaging to explore their relationships with the clinical endpoints. Our study encompasses a comprehensive range of brain imaging modalities, such as structural MRI, diffusion MRI, and resting-state fMRI. The cardiac imaging data comprise short-axis, long-axis, and aortic cine images. Volume, iron content, and percent fat were measured across 6 different abdominal organs and tissues, yielding in 11 image-derived abdominal phenotypes. Additionally, we included 8 skeleton imaging biomarkers encompassing long bone lengths as well as hip and shoulder width. (**B**). A high-level summary of our bidirectional findings. The left panel displayed all the imaging biomarkers that have been used in the study. The grey arrow demonstrates the main findings, such as the intra-brain, intra-heart, brain-heart, and brain-abdominal-organs causal connections. The right panel depicts the intricate web of causal interactions among various organs as uncovered in our study. Blue arrows signify causal relationships that involve either the heart or brain, while orange arrows represent causal connections that do not include the heart or brain. The width of an arrow corresponds to the volume of findings associated with it.

Fig. 2 Selected genetic causal effects of clinical outcomes on brain imaging biomarkers. We illustrated selected significant ($P < 5.18\times10^{-6}$) causal genetic links from clinical endpoints (Exposure) to brain imaging biomarkers (Outcome), with adjustment for multiple testing using the Bonferroni procedure. (**A**). The causal effect of Alzheimer's disease on brain imaging biomarkers. (**B**). The causal effect of dementia on brain imaging biomarkers. (**C**). The causal effect of hypertension on brain imaging biomarkers. The term 'IDP Category' is used to signify the category of imaging biomarkers, while '#IVs' stands for the number of genetic variants utilized as instrumental variables. Various MR methods and their associated regression coefficients are marked with different colors for easy identification. See **Table S1** for data resources of clinical endpoints and **Table S2** for data resources of imaging biomarkers.

Fig. 3 Selected genetic causal effects of brain imaging biomarkers on clinical endpoints. We illustrated selected significant ($P < 5.18\times10^{-6}$) causal genetic links from brain imaging biomarkers (Exposure) to clinical endpoints (Outcome), with adjustment for multiple

testing using the Bonferroni procedure. (**A**). The causal effect of brain imaging biomarkers on Alzheimer's diseases. (**B**). The causal effect of brain imaging biomarkers on dementia. The term 'IDP Category' is used to signify the category of imaging biomarkers, while '#IVs' stands for the number of genetic variants utilized as instrumental variables. Various MR methods and their associated regression coefficients are marked with different colors for easy identification. See **Table S1** for data resources of clinical endpoints and **Table S2** for data resources of imaging biomarkers.

Fig. 4 Selected genetic causal effects between heart imaging biomarkers and clinical endpoints.

(**A**). Selected significant ($P < 6.85\times10^{-6}$) causal genetic links from clinical endpoints (Exposure) to heart imaging biomarkers (Outcome) with adjustment for multiple testing using the Bonferroni procedure. (**B-C**). The heart diagram shows the region of the corresponding IDP when hypertensive diseases and hypertension are the exposure variables. (**D**). Selected significant ($P < 6.85\times10^{-6}$) causal genetic links from heart imaging biomarkers (Exposure) to clinical endpoints (Outcome) with adjustment for multiple testing using the Bonferroni procedure. (**E-G**). The heart diagram shows the region of the corresponding IDP when atrial fibrillation and flutter, heart failure and antihypertensive medication, as well as hypertension, are the outcome variables. The term 'IDP Category' is used to signify the category of imaging biomarkers, while '#IVs' stands for the number of genetic variants utilized as instrumental variables. Various MR methods and their associated regression coefficients are marked with different colors for easy identification. See **Table S1** for data resources of clinical endpoints and **Table S2** for data resources of imaging biomarkers.

Fig. 5 Selected genetic causal effects between abdominal imaging biomarkers and clinical endpoints.

We illustrated selected significant ($P < 6.69\times10^{-5}$) causal genetic links from (**A**) clinical endpoints (Exposure) to abdominal imaging biomarkers (Outcome) and (**B**) abdominal imaging biomarkers (Exposure) to clinical endpoints (Outcome) with adjustment for multiple testing using the Bonferroni procedure. The term 'IDP Category' is used to signify

the category of imaging biomarkers, while '#IVs' stands for the number of genetic variants utilized as instrumental variables. Various MR methods and their associated regression coefficients are marked with different colors for easy identification. **(C-F)**. Selected causal associations between abdominal imaging biomarkers and multi-organ diseases. See **Table S1** for data resources of clinical endpoints and **Table S2** for data resources of imaging biomarkers.

Fig. 6 Selected genetic causal effects between skeleton imaging biomarkers and clinical endpoints.

We illustrated selected significant ($P < 3.39\times10^{-5}$) causal genetic links from (**A**) clinical endpoints to (Exposure) to skeleton imaging biomarkers (Outcome) and (**B**) skeleton imaging biomarkers (Exposure) to clinical endpoints (Outcome) with adjustment for multiple testing using the Bonferroni procedure. The term 'IDP Category' is used to signify the category of imaging biomarkers, while '#IVs' stands for the number of genetic variants utilized as instrumental variables. Various MR methods and their associated regression coefficients are marked with different colors for easy identification. The skeleton diagram on the right shows the region of the corresponding IDP. See **Table S1** for data resources of clinical endpoints and **Table S2** for data resources of imaging biomarkers.

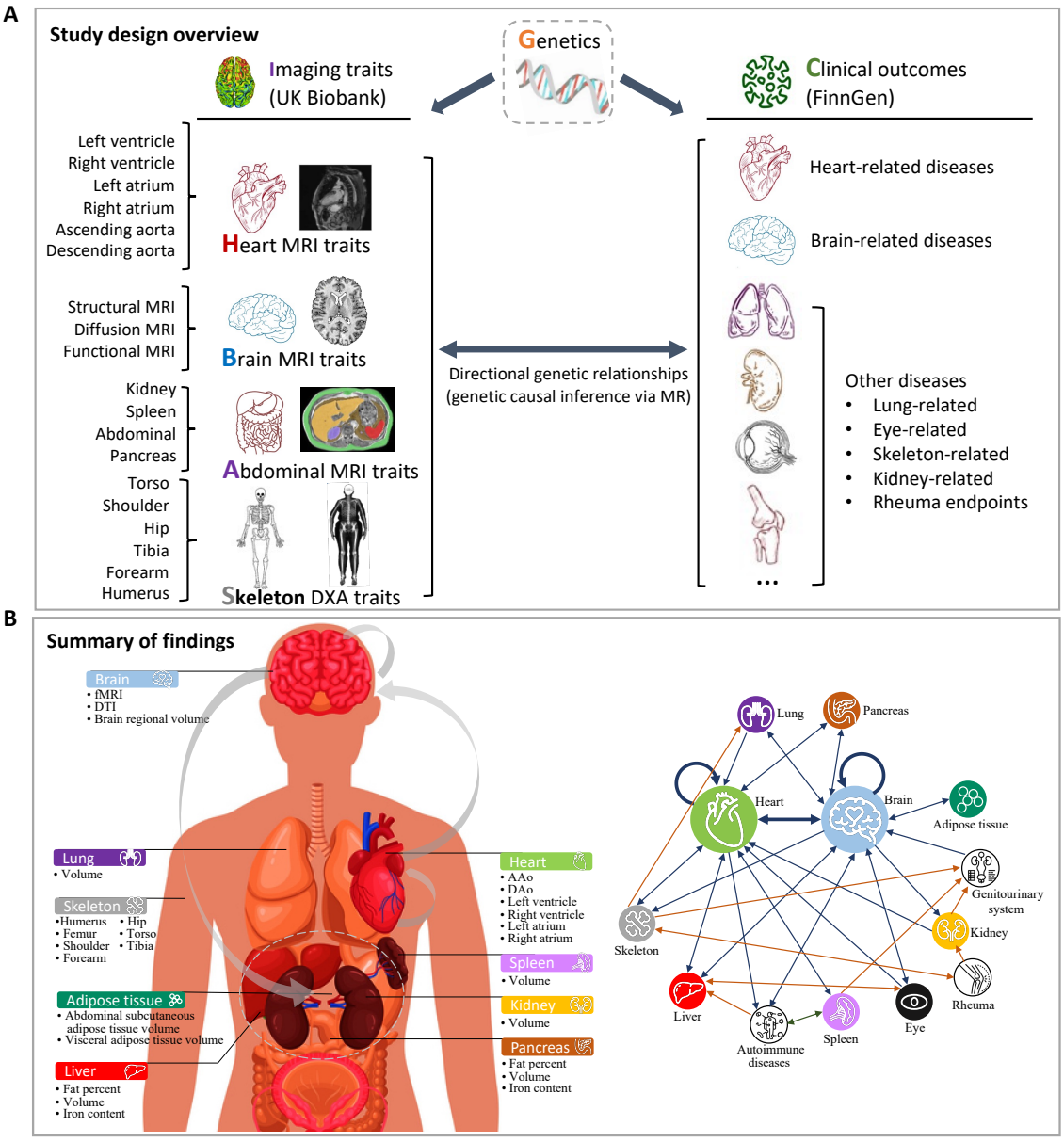
A
Study design overview
Genetics
Imaging traits
(UK Biobank)
Clinical outcomes
(FinnGen)
Left ventricle
Right ventricle
Left atrium
Right atrium
Ascending aorta
Descending aorta
Heart MRI traits
Structural MRI
Diffusion MRI
Functional MRI
Brain MRI traits
Kidney
Spleen
Abdominal
Pancreas
Abdominal MRI traits
Torso
Shoulder
Hip
Tibia
Forearm
Humerus
Skeleton DXA traits
Directional genetic relationships
(genetic causal inference via MR)
Heart-related diseases
Brain-related diseases
Other diseases
• Lung-related
• Eye-related
• Skeleton-related
• Kidney-related
• Rheuma endpoints
...
B
Summary of findings
Brain
• fMRI
• DTI
• Brain regional volume
Lung
• Volume
Skeleton
•Humerus • Hip
• Femur • Torso
• Shoulder • Tibia
• Forearm
Adipose tissue
• Abdominal subcutaneous adipose tissue volume
• Visceral adipose tissue volume
Liver
• Fat percent
• Volume
• Iron content
Heart
• AAo
• DAo
• Left ventricle
• Right ventricle
• Left atrium
• Right atrium
Spleen
• Volume
Kidney
• Volume
Pancreas
• Fat percent
• Volume
• Iron content
Lung
Pancreas
Heart
Brain
Adipose tissue
Genitourinary system
Kidney
Rheuma
Eye
Spleen
Autoimmune diseases
Liver
Skeleton

Figure 1

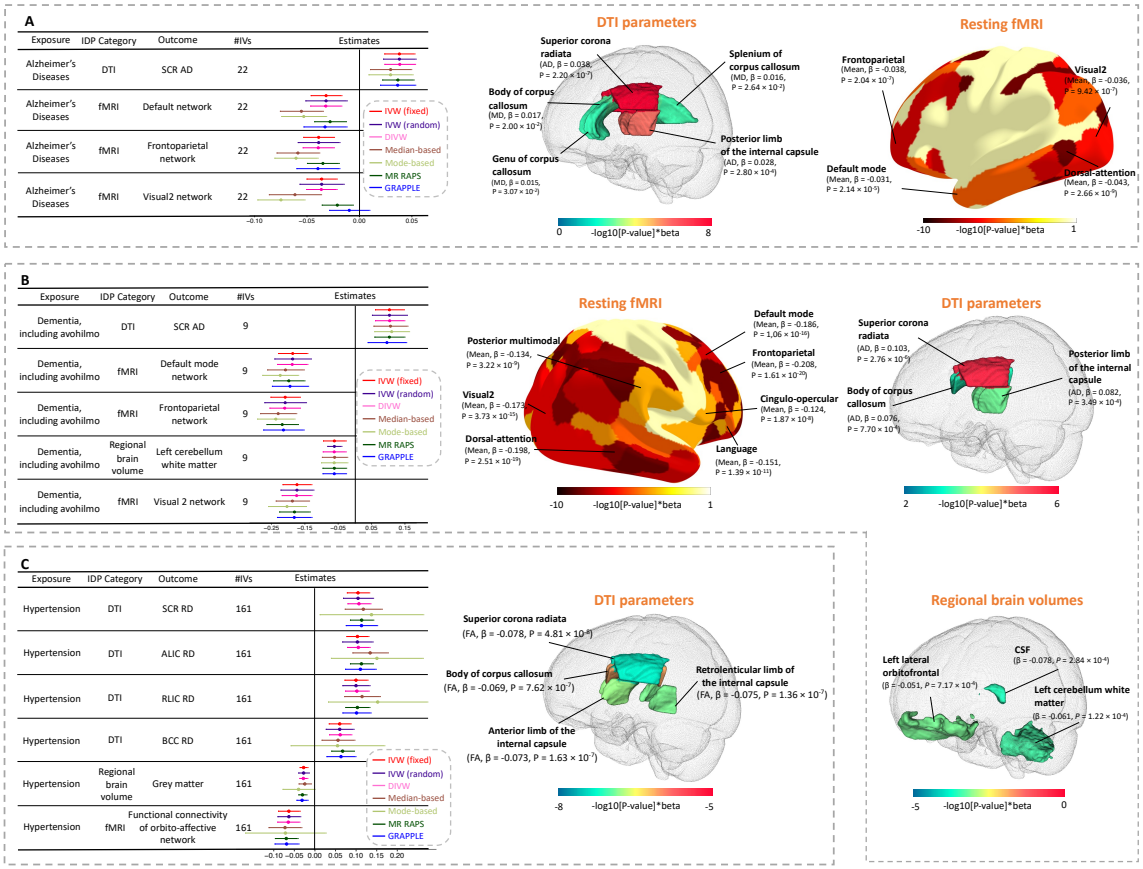
A
Exposure
IDP Category
Outcome
#IVs
Estimates
Alzheimer's Diseases
DTI
SCR AD
22
fMRI
Default network
Frontoparietal network
Visual2 network
IVW (fixed)
IVW (random)
DIVW
Median-based
Mode-based
MR RAPS
GRAPPLE
DTI parameters
Superior corona radiata
Splenium of corpus callosum
Body of corpus callosum
Posterior limb of the internal capsule
Genu of corpus callosum
0
-log10[P-value]*beta
8
Resting fMRI
Frontoparietal
Visual2
Default mode
Dorsal-attention
-10
1
B
Dementia, including avohilmo
SCR AD
9
Default mode network
Frontoparietal network
Regional brain volume
Left cerebellum white matter
Visual 2 network
Posterior multimodal
Default mode
Frontoparietal
Visual2
Cingulo-opercular
Dorsal-attention
Language
-10
1
Superior corona radiata
Posterior limb of the internal capsule
Body of corpus callosum
2
6
C
Hypertension
SCR RD
161
ALIC RD
RLIC RD
BCC RD
Grey matter
Functional connectivity of orbito-affective network
Superior corona radiata
(FA, β = -0.078, P = 4.81 × 10⁻⁴)
Body of corpus callosum
(FA, β = -0.069, P = 7.62 × 10⁻⁷)
Retrolenticular limb of the internal capsule
(FA, β = -0.075, P = 1.36 × 10⁻⁷)
Anterior limb of the internal capsule
(FA, β = -0.073, P = 1.63 × 10⁻⁷)
-8
-5
Regional brain volumes
Left lateral orbitofrontal
CSF
(β = -0.078, P = 2.84 × 10⁻⁴)
Left cerebellum white matter
(β = -0.061, P = 1.22 × 10⁻⁴)
-5
0

Figure 2

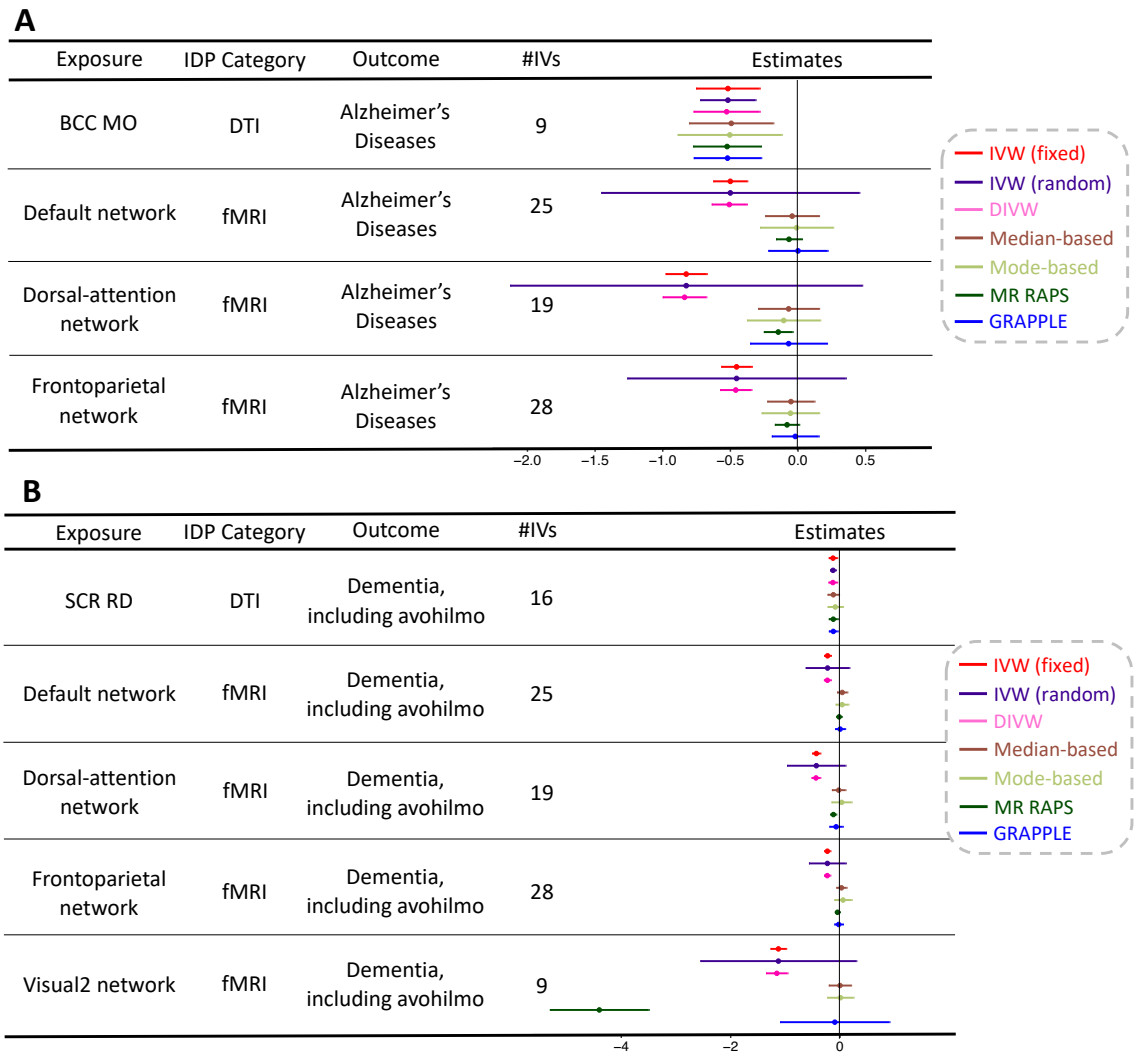
A
Exposure
IDP Category
Outcome
#IVs
Estimates
BCC MO
DTI
Alzheimer's Diseases
9
Default network
fMRI
Alzheimer's Diseases
25
Dorsal-attention network
fMRI
Alzheimer's Diseases
19
Frontoparietal network
fMRI
Alzheimer's Diseases
28
−2.0
−1.5
−1.0
−0.5
0.0
0.5
IVW (fixed)
IVW (random)
DIVW
Median-based
Mode-based
MR RAPS
GRAPPLE
B
Exposure
IDP Category
Outcome
#IVs
Estimates
SCR RD
DTI
Dementia, including avohilmo
16
Default network
fMRI
Dementia, including avohilmo
25
Dorsal-attention network
fMRI
Dementia, including avohilmo
19
Frontoparietal network
fMRI
Dementia, including avohilmo
28
Visual2 network
fMRI
Dementia, including avohilmo
9
−4
−2
0
IVW (fixed)
IVW (random)
DIVW
Median-based
Mode-based
MR RAPS
GRAPPLE

Figure 3

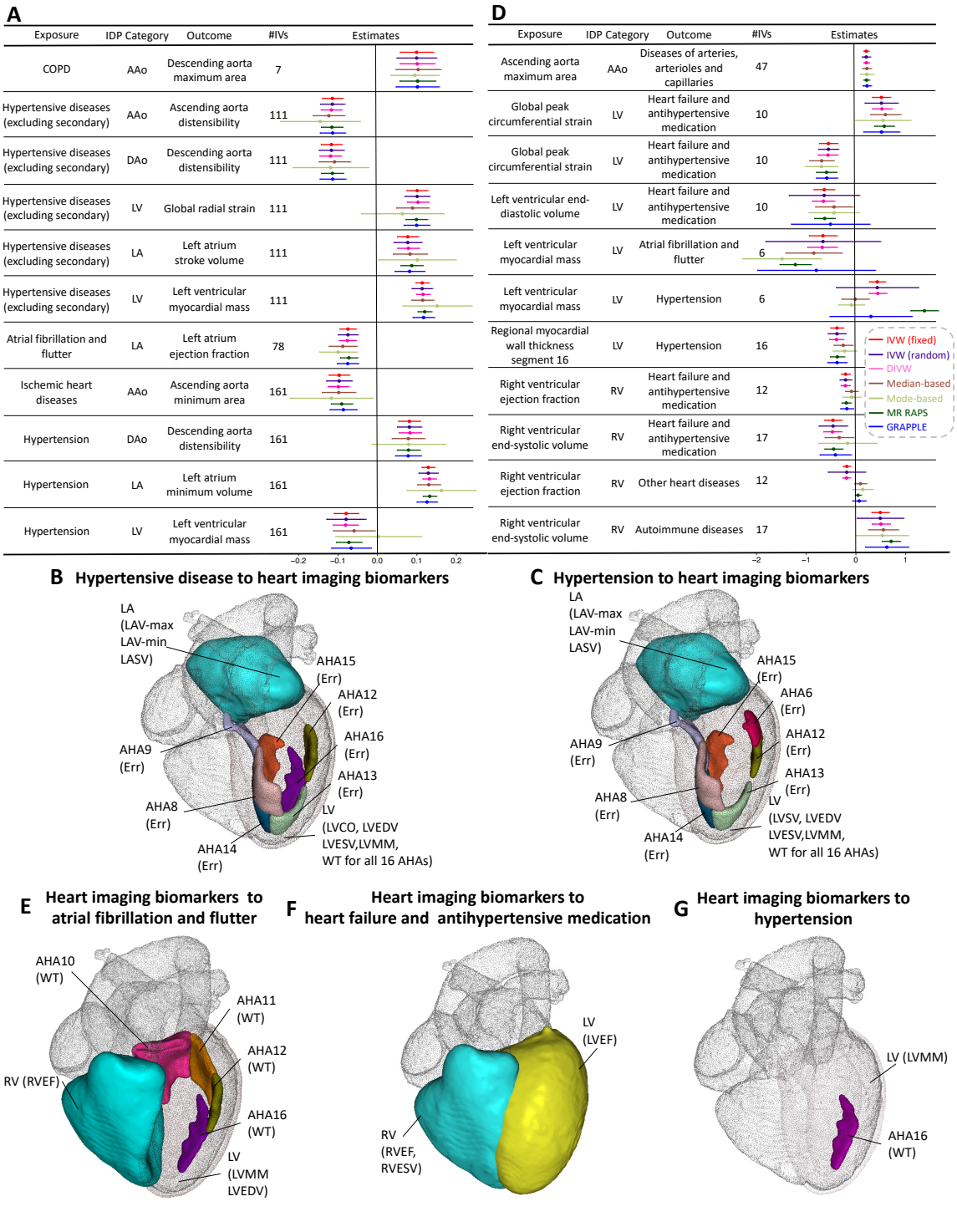
A
Exposure
IDP Category
Outcome
#IVs
Estimates
COPD
AAo
Descending aorta maximum area
7
Hypertensive diseases (excluding secondary)
AAo
Ascending aorta distensibility
111
Hypertensive diseases (excluding secondary)
DAo
Descending aorta distensibility
111
Hypertensive diseases (excluding secondary)
LV
Global radial strain
111
Hypertensive diseases (excluding secondary)
LA
Left atrium stroke volume
111
Hypertensive diseases (excluding secondary)
LV
Left ventricular myocardial mass
111
Atrial fibrillation and flutter
LA
Left atrium ejection fraction
78
Ischemic heart diseases
AAo
Ascending aorta minimum area
161
Hypertension
DAo
Descending aorta distensibility
161
Hypertension
LA
Left atrium minimum volume
161
Hypertension
LV
Left ventricular myocardial mass
161
−0.2
−0.1
0.0
0.1
0.2
D
Exposure
IDP Category
Outcome
#IVs
Estimates
Ascending aorta maximum area
AAo
Diseases of arteries, arterioles and capillaries
47
Global peak circumferential strain
LV
Heart failure and antihypertensive medication
10
Global peak circumferential strain
LV
Heart failure and antihypertensive medication
10
Left ventricular end-diastolic volume
LV
Heart failure and antihypertensive medication
10
Left ventricular myocardial mass
LV
Atrial fibrillation and flutter
6
Left ventricular myocardial mass
LV
Hypertension
6
Regional myocardial wall thickness segment 16
LV
Hypertension
16
Right ventricular ejection fraction
RV
Heart failure and antihypertensive medication
12
Right ventricular end-systolic volume
RV
Heart failure and antihypertensive medication
17
Right ventricular ejection fraction
RV
Other heart diseases
12
Right ventricular end-systolic volume
RV
Autoimmune diseases
17
−2
−1
0
1
IVW (fixed)
IVW (random)
DIVW
Median-based
Mode-based
MR RAPS
GRAPPLE
B Hypertensive disease to heart imaging biomarkers
LA (LAV-max LAV-min LASV)
AHA15 (Err)
AHA12 (Err)
AHA16 (Err)
AHA13 (Err)
LV (LVCO, LVEDV LVESV,LVMM, WT for all 16 AHAs)
AHA14 (Err)
AHA8 (Err)
AHA9 (Err)
C Hypertension to heart imaging biomarkers
LA (LAV-max LAV-min LASV)
AHA15 (Err)
AHA6 (Err)
AHA12 (Err)
AHA13 (Err)
LV (LVSV, LVEDV LVESV,LVMM, WT for all 16 AHAs)
AHA14 (Err)
AHA8 (Err)
AHA9 (Err)
E Heart imaging biomarkers to atrial fibrillation and flutter
AHA10 (WT)
AHA11 (WT)
AHA12 (WT)
AHA16 (WT)
LV (LVMM LVEDV)
RV (RVEF)
F Heart imaging biomarkers to heart failure and antihypertensive medication
LV (LVEF)
RV (RVEF, RVESV)
G Heart imaging biomarkers to hypertension
LV (LVMM)
AHA16 (WT)

Figure 4

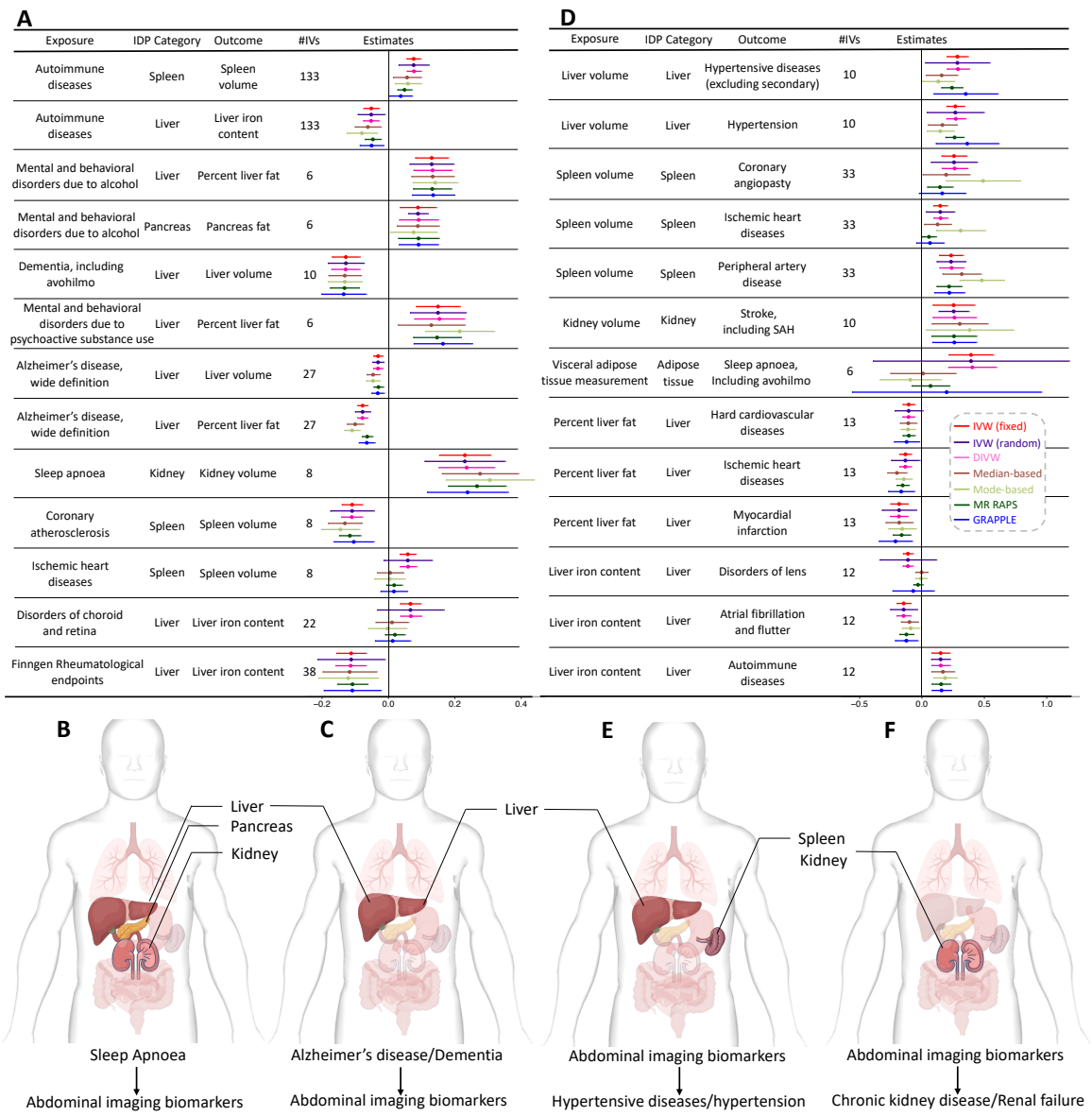
A
Exposure
IDP Category
Outcome
#IVs
Estimates
Autoimmune diseases
Spleen
Spleen volume
133
Autoimmune diseases
Liver
Liver iron content
133
Mental and behavioral disorders due to alcohol
Liver
Percent liver fat
6
Mental and behavioral disorders due to alcohol
Pancreas
Pancreas fat
6
Dementia, including avohilmo
Liver
Liver volume
10
Mental and behavioral disorders due to psychoactive substance use
Liver
Percent liver fat
6
Alzheimer's disease, wide definition
Liver
Liver volume
27
Alzheimer's disease, wide definition
Liver
Percent liver fat
27
Sleep apnoea
Kidney
Kidney volume
8
Coronary atherosclerosis
Spleen
Spleen volume
8
Ischemic heart diseases
Spleen
Spleen volume
8
Disorders of choroid and retina
Liver
Liver iron content
22
Finngen Rheumatological endpoints
Liver
Liver iron content
38
−0.2
0.0
0.2
0.4
D
Exposure
IDP Category
Outcome
#IVs
Estimates
Liver volume
Liver
Hypertensive diseases (excluding secondary)
10
Liver volume
Liver
Hypertension
10
Spleen volume
Spleen
Coronary angiopasty
33
Spleen volume
Spleen
Ischemic heart diseases
33
Spleen volume
Spleen
Peripheral artery disease
33
Kidney volume
Kidney
Stroke, including SAH
10
Visceral adipose tissue measurement
Adipose tissue
Sleep apnoea, Including avohilmo
6
Percent liver fat
Liver
Hard cardiovascular diseases
13
Percent liver fat
Liver
Ischemic heart diseases
13
Percent liver fat
Liver
Myocardial infarction
13
Liver iron content
Liver
Disorders of lens
12
Liver iron content
Liver
Atrial fibrillation and flutter
12
Liver iron content
Liver
Autoimmune diseases
12
−0.5
0.0
0.5
1.0
IVW (fixed)
IVW (random)
DIVW
Median-based
Mode-based
MR RAPS
GRAPPLE
B
Liver
Pancreas
Kidney
Sleep Apnoea
Abdominal imaging biomarkers
C
Liver
Alzheimer's disease/Dementia
Abdominal imaging biomarkers
E
Spleen
Kidney
Abdominal imaging biomarkers
Hypertensive diseases/hypertension
F
Abdominal imaging biomarkers
Chronic kidney disease/Renal failure

Figure 5

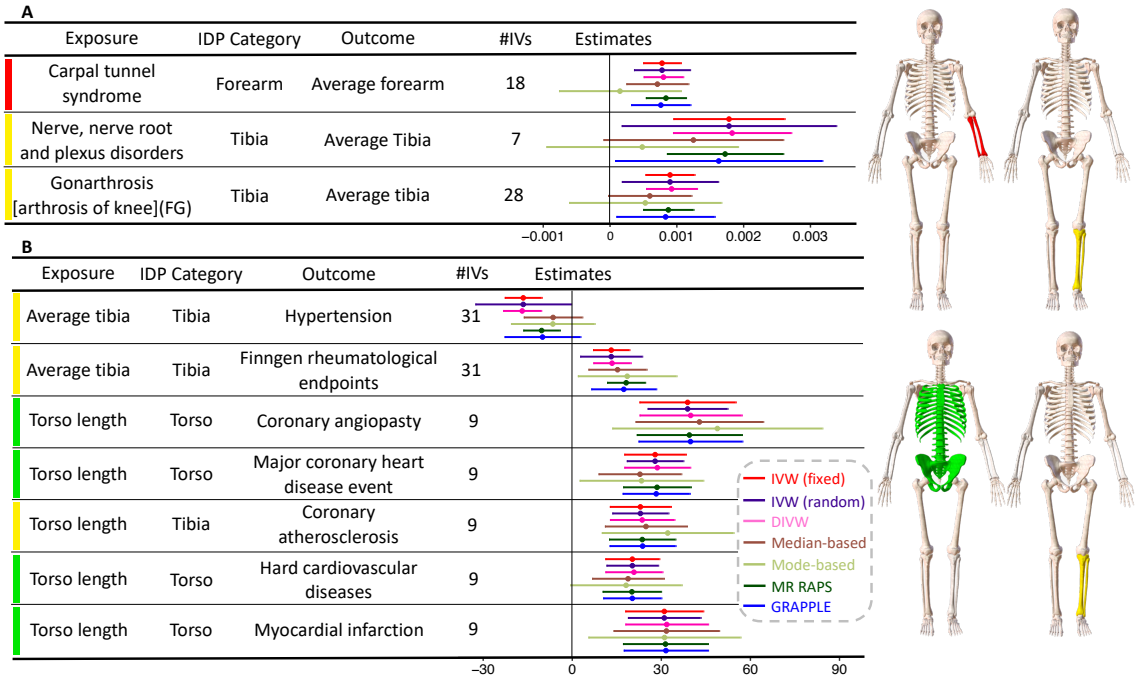
A
Exposure
IDP Category
Outcome
#IVs
Estimates
Carpal tunnel syndrome
Forearm
Average forearm
18
Nerve, nerve root and plexus disorders
Tibia
Average Tibia
7
Gonarthrosis [arthrosis of knee](FG)
Tibia
Average tibia
28
−0.001
0
0.001
0.002
0.003
B
Exposure
IDP Category
Outcome
#IVs
Estimates
Average tibia
Tibia
Hypertension
31
Average tibia
Tibia
Finngen rheumatological endpoints
31
Torso length
Torso
Coronary angiopasty
9
Torso length
Torso
Major coronary heart disease event
9
Torso length
Tibia
Coronary atherosclerosis
9
Torso length
Torso
Hard cardiovascular diseases
9
Torso length
Torso
Myocardial infarction
9
−30
0
30
60
90
IVW (fixed)
IVW (random)
DIVW
Median-based
Mode-based
MR RAPS
GRAPPLE

Figure 6